bioRxiv preprint doi: https://doi.org/10.1101/2022.10.03.510635; this version posted October 5, 2022. The copyright holder for this preprint (which was not certified by peer review) is the author/funder, who has granted bioRxiv a license to display the preprint in perpetuity. It is made available under aCC-BY 4.0 International license.

Suppression of Betacellulin expression is a key mechanism for omega-3 fatty acid mediated attenuation of nonalcoholic steatohepatitis

Jyothi Padiadpu[1], Manuel Garcia-Jaramillo[4#,] Nolan Newman[1#], Jacob Pederson[2#], Richard Rodrigues[1,6], Zhipeng Li[2], Sehajvir Singh[1], Philip Monnier[1], Giorgio Trinchieri[6], Kevin Brown[1,5], Amiran K. Dzutsev[6], Natalia Shulzhenko[2]*, Donald B. Jump[3]*, Andrey Morgun[1]*

Affiliations:

[1] College of Pharmacy, Oregon State University, Corvallis, OR, USA.

[2] Veterinary Medicine, Oregon State University, Corvallis, OR, USA.

[3] Nutrition Program, School of Biological and Population Health Sciences, Linus Pauling Institute, Oregon State University, Corvallis, OR, USA

[4]Department of Environmental and Molecular Toxicology, Oregon State University, Corvallis, OR, USA.

[5]School of Chemical, Biological, and Environmental Engineering, Oregon State University, Corvallis, OR, USA.

[6]Cancer and Inflammation Program, Center for Cancer Research, National Cancer Institute, National Institutes of Health, Bethesda, MD, USA.

*Co-senior correspondence to: donald.jump@oregonstate.edu or Natalia.Shulzhenko@oregonstate.edu or Andriy.Morgun@oregonstate.edu

[#] These authors contributed equally to this work

Abstract

Nonalcoholic steatohepatitis (NASH) is currently the only prevalent metabolic disease with no FDA-approved treatment strategy. Supplementation of ω3 polyunsaturated fatty acids (PUFA) represent a promising treatment as it can attenuate fibrosis and inflammation, but the mechanisms are poorly defined. We employed a causal inference approach for multi-omics network analysis which revealed critical cellular and molecular processes responsible for the effects of ω3 PUFA (Docosahexaenoic acid, DHA; Eicosapentaenoic acid, EPA) in a preclinical mouse model of NASH. Because NASH is one of the leading causes of liver cancer, we also performed a meta-analysis of 7 cancer datasets and integrated these results with the mouse gene expression network. The overlap of the NASH network with meta-analysis identified betacellulin (BTC)-EGFR-ERBB as a central pathway of hepatocellular carcinoma. In mice, DHA inhibits this pathway. Using two cell lines, we confirmed that BTC acts at several levels of pathogenesis by: 1) promoting proliferation of quiescent hepatic stellate cells; 2) stimulating transforming growth factor–β2 (TGFβ-2), which increases collagen production, and 3) upregulation of integrins in macrophages together with TLR2/4 agonists. Strikingly, these pathogenic processes were attenuated by DHA and to a much lesser degree by EPA. We also found that DHA restores hepatic cardiolipin precursors and mitochondrial pathways. Together, our results suggest that inhibition of BTC by DHA is a key mechanism behind its beneficial effects on liver health, and that administration of DHA may prevent progression of NASH to liver cancer by averting the BTC-EGFR-ERBB pathway.

bioRxiv preprint doi: https://doi.org/10.1101/2022.10.03.510635; this version posted October 5, 2022. The copyright holder for this preprint (which was not certified by peer review) is the author/funder, who has granted bioRxiv a license to display the preprint in perpetuity. It is made available under aCC-BY 4.0 International license.

One Sentence Summary: Multi-omics network analysis reveals suppression of Betacellulin expression is a key mechanism for ω3 PUFA mediated attenuation of nonalcoholic steatohepatitis

Introduction

Metabolic diseases associated with obesity have increased to epidemic proportions in recent years and are one of the leading causes of morbidity and mortality (*1*, *2*). Metabolic-associated fatty liver disease (MAFLD) or nonalcoholic steatohepatitis (NASH), type 2 diabetes and cardiovascular diseases are all associated with obesity and a sedentary lifestyle (*3*, *4*). About 80 million adults and 13 million children are obese in the US alone. Among these, 60 percent of patients with body mass index greater than 30 have evidence of liver steatosis (*2*, *5*). NASH is a progressive form of nonalcoholic fatty liver disease (NAFLD) and is a major risk factor for cirrhosis, hepatocellular carcinoma (HCC) and liver failure. While treatments to manage the co-morbidities associated with NASH, i.e., obesity and type 2 diabetes are available, NASH has no specific FDA-approved treatment. Thus, lifestyle modifications and dietary interventions are the only current options available to NASH patients. Most if not all drugs which targeted individual molecules or specific pathways have failed to significantly improve the NASH patient (*2*, *6-8*). This modern strategy that has been effective in the treatment of some diseases might not be adequate for NAFLD/NASH therapy because it does not address entirely the complexity of this disease and may miss the master regulators involved in disease onset and progression.

Because omega-3 (ω3) polyunsaturated fatty acids (PUFA) were consistently lower in livers of NASH patients when compared to healthy patients or patients with benign steatosis (*9*, *10*), we hypothesized that dietary supplementation with these fatty acids would restore liver functions. Indeed, this strategy was very successful in a preclinical mouse model, not only reducing liver steatosis but also in attenuating western diet-induced hepatic fibrosis (*5*, *11*, *12*). Moreover, ω3 fatty acid treatment of children and adults with NAFLD have demonstrated these dietary lipids reduce hepatic steatosis and hepatic injury (*13*, *14*). While it is well established that ω3 PUFA have the capacity to regulate hepatic mechanisms controlling fatty acid synthesis and oxidation, as well as inflammation, it is less clear if these pathways form the extent of ω3 fatty acid regulation of hepatic function (*15*). Despite several studies demonstrating the therapeutic effects of ω3 PUFA in NAFLD/NASH models the mechanism of action has been elusive. Nevertheless, it is important to note that many studies demonstrated diverse effects of ω3 in the liver ranging from immune-modulatory activities(*16*) and improvement of oxidative stress (*17*) to structural effects related to incorporation of phospholipids into the mitochondrial membrane, altogether with potentially positive impact on liver function. In addition to the effects of ω3 PUFA on hepatic cells, recent studies suggest that ω3 PUFA can alter gut microbiota, a known

bioRxiv preprint doi: https://doi.org/10.1101/2022.10.03.510635; this version posted October 5, 2022. The copyright holder for this preprint (which was not certified by peer review) is the author/funder, who has granted bioRxiv a license to display the preprint in perpetuity. It is made available under aCC-BY 4.0 International license.

player in the pathogenesis of NAFLD/NASH (*18*). Furthermore, preclinical and clinical studies demonstrated that docosahexaenoic acid (DHA, 22:6, ω3) might be a more efficient agent than eicosapentaenoic acid (EPA, 20:5, ω3) in preventing and treating NAFLD (*11-13*).

Thus, while there are many studies describing different molecular and cellular effects of ω3 fatty acids (*19-24*) and some evidence that they may be an efficient therapy for NAFLD/NASH the key mechanisms of their impact in improving liver health are still unknown.

Because the preclinical data indicates the potential for specific ω3 PUFA to improve liver health, the known mechanisms for ω3 PUFA action were likely insufficient to account for the anti-fibrotic effect of these fatty acids on the liver. As such, we used a comprehensive unbiased approach to identify novel mechanisms. Accordingly, we evaluated the liver transcriptome, metabolome and lipidome and used causal inferences via network analysis to identify prospective mechanism operating in the diseased liver that were restored by EPA and/or DHA. We also performed meta-analysis of human liver cancer to understand which aspects of NASH pathogenesis leads to HCC.

The main finding of this undertaking established that betacellulin (BTC), one of several agonists of EGFRs, as a master regulatory molecule that is downregulated by ω3 PUFA in the NASH liver. We further confirmed the impact of BTC by in cell culture experiments that established TGFβ-2 and integrins are the main downstream molecular targets of BTC in human hepatic stellate cells and macrophage, respectively. As such, our study disclosed an entirely novel mechanism for ω3 fatty acid control of hepatic function and its beneficial action against detrimental molecular events in the liver leading to NASH.

Results

DHA reverses the effects of WD more effectively than EPA

We performed a comprehensive analysis of molecular changes contributing to prevention of NAFLD/NASH by ω3 PUFA, namely docosahexaenoic (DHA, 22:6, ω3) and Eicosapentaenoic acid (EPA, 20:5, ω3). We evaluated transcriptomic, metabolomic and lipidomic changes caused by DHA and EPA in the whole tissue liver samples from *Ldlr* $^{-/-}$ mice fed a western diet (WD) with the addition (or not) of DHA or EPA (*12*) (**Figure 1A-C,** Suppl Table S1**)**. To focus our analysis on disease features corrected by ω3s, we first established which changes induced by WD were reversed by DHA or EPA treatment (see M&M for details). We then established four categories of parameters: 1) regulated by DHA only (e.g., Cd36, **Figure 1D** top left); 2) regulated by EPA only (e.g., Notch2, **Figure 1D** top right); 3) regulated similarly by DHA and EPA (e.g., Cx3Cr1, **Figure 1D** bottom left); 4) not regulated by either DHA or EPA (e.g., Egfr, **Figure 1D** bottom right). Although there was a large overlap between the effects of each ω3, overall, DHA showed stronger effects than EPA in restoring alterations caused by WD. Specifically, while both EPA and DHA showed similar effects on 19% of the genes affected by disease, DHA alone reversed more genes (11%) than EPA alone (3%), (**Figure 1B, C**). In line with this result, focusing on genes regulated by both fatty acids (DHA and EPA) we observed

bioRxiv preprint doi: https://doi.org/10.1101/2022.10.03.510635; this version posted October 5, 2022. The copyright holder for this preprint (which was not certified by peer review) is the author/funder, who has granted bioRxiv a license to display the preprint in perpetuity. It is made available under aCC-BY 4.0 International license.

more pronounced changes by DHA than EPA ($p<0.0001$) (**Figure 1E, Figure S1A, B**). The genes upregulated and reversed by DHA were enriched for several functional categories: mitochondrial organization, translation, and energy derivation by oxidation of organic compounds were among the most prominent pathways affected. Regulation of cytokine production was the top enriched pathway among the downregulated genes (**Figure 1F**). Thus, the first step of transcriptome analysis indicated that DHA had a stronger effect than EPA in reversing damage inflicted by WD on the liver potentially by restoring mitochondrial tissue function and inhibiting inflammation.

In the second largest omics data represented by lipidomes, we did not see differences in the number of lipids regulated by DHA or EPA. We detect a significantly stronger effect on lipids regulated by DHA versus lipids regulated by EPA (**Figure S1C**). Analysis of anthropometric features and plasma biochemicals also showed a more pronounced effect by DHA than EPA as previously reported (*12*) (Figure 1A). Overall, DHA demonstrated stronger effects than EPA in reversing WD caused alterations to both gene expression and lipid concentrations.

Figure 1. NASH mouse model outline with all expression/omics data, DHA/EPA treatment effects on outcome.

A. All omics data collected and shown in Fig 1A bar graph and its associated table was acquired using samples (N = 8/treatment group) from a preclinical NASH prevention study previously described (*11, 12, 25*). The comparison of the western diet + olive oil (WD+O) group verses reference diet (chow, RD) group showing the differentially expressed genes or parameters with a P-value <0.05 and FDR <10% and those that have treatment effect reversal uniquely by DHA (blue), EPA (orange) or similar in both EPA&DHA (green).

B. Heatmap of differentially expressed genes in WD+O vs. RD fed mice and organized by treatment effect category: DHA, EPA, or DHA & EPA. Data shown are the geometric mean expression for each gene per each treatment group. Row max is displayed as red, row min is displayed as blue.

C. Heatmap of parameters (lipids and metabolites) in WD+O vs. RD fed mice and organized by treatment effect category (DHA, EPA, or DHA &EPA) that are significant at P-value <0.05 and FDR <0.1. Data shown are a geometric mean of each parameter measurement for each treatment group. Row max: red, row min: blue.

D. Shown are selected representatives (Cd36, Notch2, Cx3cr1 & Egfr) from each category according to treatment effect (top left: DHA, top right: EPA, bottom left: EPA & DHA, bottom right: no treatment effect). Shown here is an example of one gene from each category (mean +/- SD). (N=8 mice/treatment group, One-way ANOVA, with multiple comparisons test with WD+O, ns (not significant), *p<0.05, ** p<0.001, *** p<0.005, ****p<0.0001).

E. Scatterplot of fold change differences between WD+O and DHA or EPA treated mice with number of genes regulated by DHA (Blue) or EPA (Orange) displayed. (Pearson's Chi-squared test, ****p<0.0001).

F. Top enriched biological process changed by DHA treatment. Top + Blue bars: Induction by DHA, Bottom + Green bars; Repression by DHA. Bars show -log10(p-value) transformed values for visualization.

bioRxiv preprint doi: https://doi.org/10.1101/2022.10.03.510635; this version posted October 5, 2022. The copyright holder for this preprint (which was not certified by peer review) is the author/funder, who has granted bioRxiv a license to display the preprint in perpetuity. It is made available under aCC-BY 4.0 International license.

Figure 1

A

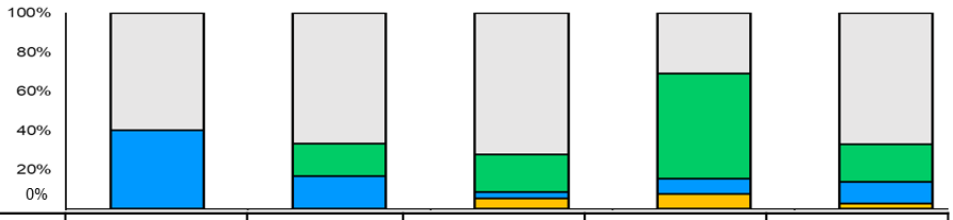

	Anthropometric	Plasma biochemicals	Metabolites	Lipidomics	RNA
EPA	0	0	3	31	193
DHA	2	2	2	32	816
EPA&DHA	0	2	11	223	1403
No treatment effect	3	8	42	129	4948

B

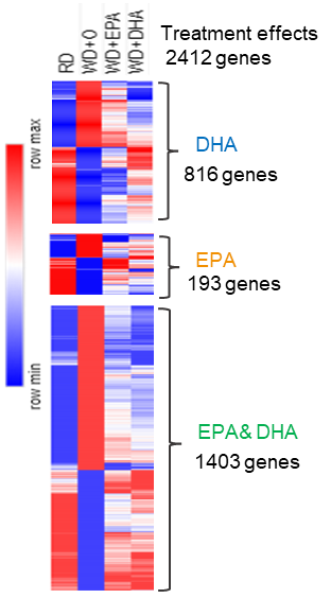

C

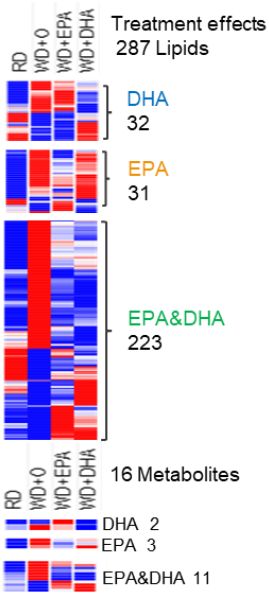

D

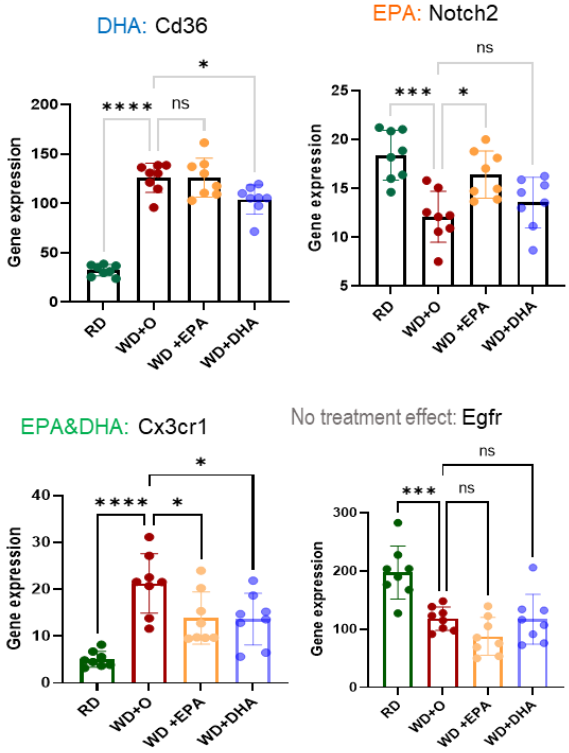

E

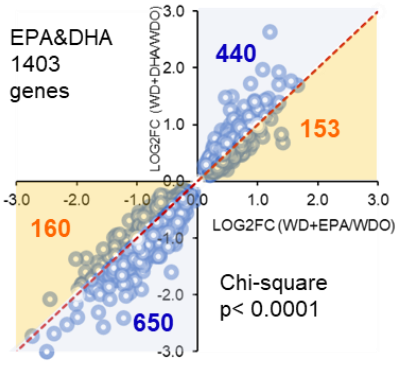

F

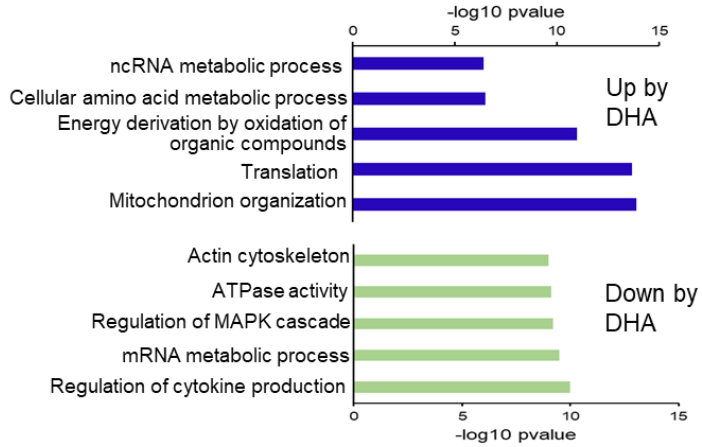

bioRxiv preprint doi: https://doi.org/10.1101/2022.10.03.510635; this version posted October 5, 2022. The copyright holder for this preprint (which was not certified by peer review) is the author/funder, who has granted bioRxiv a license to display the preprint in perpetuity. It is made available under aCC-BY 4.0 International license.

Mapping effects of ω3 onto multi-omic network model of NASH and its cellular components

To investigate how changes in different omics data relate to each other and which of the effects are contributing to the beneficial effects of ω3 PUFA, we have reconstructed a multi-omic network model of NAFLD/NASH and mapped ω3 PUFA effects into this model (Figure S2A). After filtering out data features that did not pass statistical(*26*) and causality(*27*) criteria thresholds (see materials and methods), the multi-omics network consisted of 6743 nodes connected by 80811 edges. Specifically, the network includes 6346 gene transcripts, 5 anthropometric nodes, 11 plasma biochemicals, 357 lipids, and 24 metabolites (**Figure 2A**). We next identified clusters (sub-networks) and using functional enrichment analyses found that different subnetworks were enriched in different pathways, including mitochondrial organization, myeloid leukocyte activation, cell and mitochondrial membrane fluidity, remodeling, signaling and energy metabolism. It also included processes such as macromolecule catabolic process and fatty acid metabolic process (**Figure 2A,** Suppl Table S1). It is known that multiple cell types in the liver contribute to NASH pathogenesis (*28-30*). However, which cells are responding to DHA treatment has not been systematically studied. Therefore, we mapped genes regulated by ω3 PUFA to cell type information using a previously published single cell RNA-seq dataset generated from diet-induced NASH mouse livers (see materials and methods) (*28*). Among different cell types, most of the genes were assigned to one of macrophage subpopulations (MF1, 585 genes and MF2, 1455 genes), followed by hepatocytes, cholangiocytes and hepatic stellate cells (522, 365 and 192 genes respectively) (**Figure 2B**). In line with our initial observation (Figure 1A), we found that DHA reversed expression of a larger number of genes than EPA irrespectively of the cell type (**Figure 2B**).

We next investigated if the network's cell-cell connectivity agrees with the primary beneficial role of DHA. We inferred the cell-cell connectivity based on genes assigned to a particular cell type and the information flow between genes in the transcriptome network (**Figure S2B**). For this, we calculated bipartite betweenness centralities (BiBC)(*26, 31*), a network topological metric, that reflects a potential causal contribution of a node (gene, metabolite, etc.) for transmitting information flow. To account for all possible cellular interactions, we calculated BiBCs across all pair-wise cell-cell connections. As expected, DHA and DHA&EPA regulated genes had higher BiBCs than EPA-regulated or those unaffected by either fatty acid (**Figure 2C; Figure S2C**). This result shows not only that DHA controls more genes than EPA in the liver (Figure 1), DHA-regulated genes most likely have higher causal contribution to cell-cell interactions in the liver during NAFLD/NASH.

bioRxiv preprint doi: https://doi.org/10.1101/2022.10.03.510635; this version posted October 5, 2022. The copyright holder for this preprint (which was not certified by peer review) is the author/funder, who has granted bioRxiv a license to display the preprint in perpetuity. It is made available under aCC-BY 4.0 International license.

Figure 2

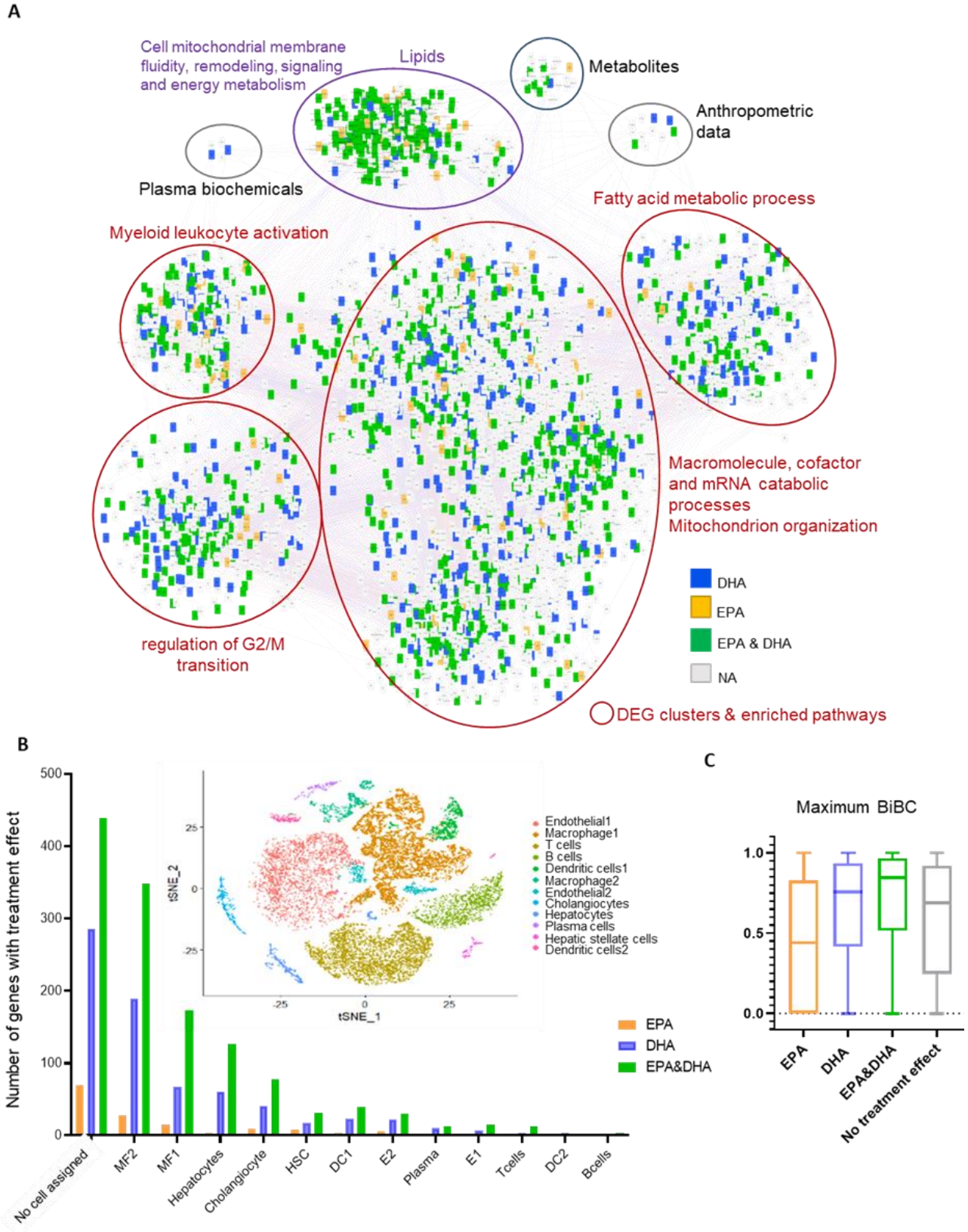

bioRxiv preprint doi: https://doi.org/10.1101/2022.10.03.510635; this version posted October 5, 2022. The copyright holder for this preprint (which was not certified by peer review) is the author/funder, who has granted bioRxiv a license to display the preprint in perpetuity. It is made available under aCC-BY 4.0 International license.

Figure 2. Multi-omics network (NW) reconstructed to model NASH *in vivo*
A. The cytoscape visualization of the network has nodes representing genes (oval), lipids (triangle, hexagon or octagon), metabolites (diamond), plasma biochemical (parallelogram), and anthropometric data (rectangle) and edges representing correlation in grey. The nodes are colored based on their treatment effect category membership, with DHA (blue), EPA&DHA (green), EPA (orange) and no category (grey). Network clusters are based on infomap modules characterized by gene and lipids functional enrichment.
B. Bar plot of number of NW genes from each treatment category (DHA (blue), EPA (orange), or EPA&DHA (green)) with assignment to a given cell type. Subplot: figure shows t-SNE plot with all cell type clusters from a reanalyzed NASH mouse single cell RNA-seq dataset (*28*) used in our study to assign cell type information. MF-macrophages, DC- dendritic cells, HSC- hepatic stellate cells and E-endothelial cells.
C. Box plot of maximum cell-cell interaction BiBC for the genes belonging to each treatment effect category (DHA (blue), EPA&DHA (green), EPA (orange) and no category (grey) shown in the graph. From the network cell-cell BiBC analysis, genes regulated by DHA have higher median BiBC which indicates a higher causal contribution to cell-cell communication than genes regulated by EPA.

Interrogation of multi-omics network finds DHA/EPA among key lipid drivers of alterations caused by WD and reveals mitochondrial cardiolipin pathway at the center of lipidome-transcriptome interactions.

Thus far, our analyses comprise inferences mostly derived from the transcriptomic component of the network. However, there is an undisputable role of lipids in NASH, including the fact that ω3 PUFA have a remarkable effect in protecting against the disease. In order to find most critical lipids/metabolites potentially involved in control of transcriptomics alterations we again took advantage of the fact that a node's topological parameters in a co-variation network (degree and BiBCs) are highly reflective of that node's potential causal contribution. Specifically, nodes of high degree (also called hubs) usually represent master regulators of a part of the large network (clusters or subnetworks) in which these hubs are situated (*32*, *33*). High ranked BiBC nodes would represent factors mediating impact of one part (e.g., module/cluster) of a network on another (*31*, *34*). Thus, we selected nodes from lipids/metabolites that are part of the network, top ranked in BiBC (top 10%) and have high degree (top 10%), also regulated by DHA (M&M).

Among the lipids that would fulfill these criteria (representing less than 2% of total lipids detected in our data), there were triglycerides, sphingomyelins, and cardiolipin precursors (**Figure 3A-C**). Two out of five lipids were triglycerides containing EPA and DHA (TG 58:11 and TG 60:10) as acyl chains (Figure 3A), while only 7 lipids out of 357 molecules had similar chemical composition (i.e., TG containing EPA/DHA) were detected by our lipidomic assay, thus, making finding this at random virtually impossible ($p<0.0001$). Remarkably, our analysis recognized as key regulators the very same fatty acids (EPA and DHA) whose depletion in the

bioRxiv preprint doi: https://doi.org/10.1101/2022.10.03.510635; this version posted October 5, 2022. The copyright holder for this preprint (which was not certified by peer review) is the author/funder, who has granted bioRxiv a license to display the preprint in perpetuity. It is made available under aCC-BY 4.0 International license.

liver is known as one of critical factors of NAFLD/NASH pathogenesis (*5, 9, 10*) and which were coincidently used as a therapy in the current study. Interestingly, we also observed the restoration Elovl5 (Figure S3B), a key enzyme involved in the elongation of mono- and polyunsaturated fatty acids (*35*). Together, these results validate the implemented network analysis for lipidomic data (previously used and experimentally validated only for other omics (*31, 34*), thereby reinforcing a potential importance of other lipids highly ranked in our analysis. Among top ranked lipids were phosphatidic acid (PA) and phosphatidyl glycerol (PGs) such as PA 38:6, PG 38:6, and PG 38:3; all of these lipids are precursors of cardiolipin (unique mitochondrial membrane phospholipid) and restored by DHA (**Figure 3C**). Further, mitochondrial membrane sphingomyelins SM d40:1 and SM d42:2 were also identified as possible critical compounds regulated by DHA (SM d40:1) or by both EPA and DHA (SM d42:2). Since neither EPA nor DHA are components of hepatic sphingolipids, their effects are on mechanisms controlling SM synthesis and/or turnover.

Motivated by these findings, we further investigated the transcriptomic data most connected to mitochondrial lipids (**Figure S3A-B**). First, interrogations for key driver genes (i.e. high degree and high BiBC genes) revealed several previously established enzymes involved in the cardiolipin pathway (e.g. Lpgat1, Prelid3b and Taz (Tafazzin) (*36-38*) **(Figure S2D, S3A).** Importantly, the expression of these genes was restored only by DHA treatment but not EPA (**Figure 3C**).

These genes belonged to a previously identified subnetwork (**Figure 2A**), named "Mitochondrial organization and mitochondrial envelope". To further focus on details of this pathway we expanded this subnetwork by including 10 additional genes in the pathway that did not previously make it into the NASH network (see M&M). This gene-lipid module included 18 genes corresponding to enzymes and 28 lipids, altogether comprising the entire cardiolipin pathway. We found that important precursor phosphatidylglycerols and phosphatidic acids were connected to cardiolipin synthesis and remodeling enzymes (**Figure 3D,** Suppl Table S2), supporting cross regulation between enzymes restored by DHA and lipids forming cardiolipins in mitochondria.

We next investigated which cells are enriched in mitochondrial genes whose expression was restored by DHA. In addition to hepatocytes (as expected), we also observed strong enrichment in macrophages (Figure S3C, S3D) suggesting an important role for DHA-improved mitochondrial function in immune cells. Overall, the results concerning lipid-transcriptome interactions point to restoration of mitochondrial function by membrane remodeling via cardiolipin synthesis as a critical mechanism of NASH prevention by DHA.

bioRxiv preprint doi: https://doi.org/10.1101/2022.10.03.510635; this version posted October 5, 2022. The copyright holder for this preprint (which was not certified by peer review) is the author/funder, who has granted bioRxiv a license to display the preprint in perpetuity. It is made available under aCC-BY 4.0 International license.

Figure 3

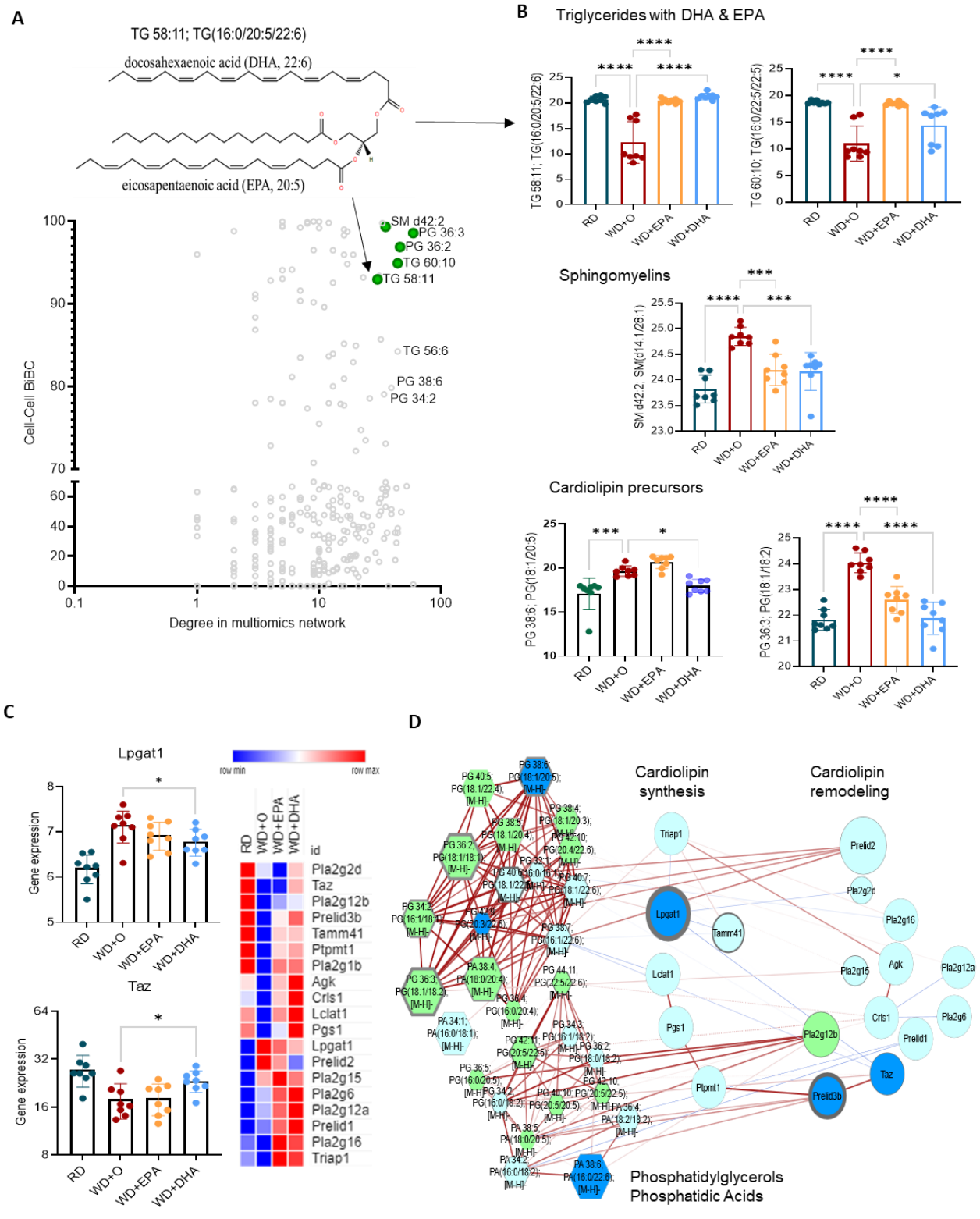

bioRxiv preprint doi: https://doi.org/10.1101/2022.10.03.510635; this version posted October 5, 2022. The copyright holder for this preprint (which was not certified by peer review) is the author/funder, who has granted bioRxiv a license to display the preprint in perpetuity. It is made available under aCC-BY 4.0 International license.

Figure 3. NW interrogation with treatment effects on lipid/metabolites and mitochondrial membrane cardiolipin model

A. The scatterplot shows the network cell-cell BiBC verses node degree for the top hepatic lipids in the NASH network. The figure insert is the structural representation of the lipid TG58:11(TG 16:0/20:5/22:6) with DHA and EPA as two of its acyl chains from the NASH prevention study. These top hepatic lipids are shown with treatment effect category EPA&DHA (green).

B. Abundance of top BiBC lipids from triglycerides, sphingolipids and phosphatidylglycerol (a precursor to mitochondrial cardiolipin. Data are mean +/- SD, N=8 mice/treatment group,
(Ordinary One-way ANOVA, multiple comparisons test with WD+O, ns (not significant), *p<0.05, ** p<0.001, *** p<0.005, ****p<0.0001).

C. Treatment effects on expression of Lpgat1 and Taz as well as multiple transcripts encoding proteins involved in cardiolipin synthesis and remodeling. Data are mean +/- SD, N=8 mice/treatment group. (Ordinary One-way ANOVA, with Dunnett's multiple comparisons test with WD+O, ns (not significant), *p<0.05, ** p<0.001, *** p<0.005, ****p<0.0001).

D. A subnetwork representing the cardiolipin synthesis and remodeling pathway in the NASH Network model. The nodes are ovals for genes and hexagons for PAs and PGs. Node color represents treatment effect category for DHA (blue), EPA&DHA (green), EPA (orange) and No Effect (light blue). Edge color represents direction of correlation (red is positive, blue if negative) and thickness denotes absolute value effect size. The node outline thickness increases with increasing BiBC.

Cancer meta-analysis indicates DHA has the potential to reverse NASH to liver cancer transition

The most dangerous consequence of NASH is a progression to liver cirrhosis and cancer in humans. Although ω3 PUFA have been studied as a potential prevention strategy for colorectal cancer progression and other cancers (*39*, *40*), there is still little understanding which cancer pathways can be inhibited by these fatty acids. As a next step, we mapped the molecular model of beneficial transcriptome alterations by DHA in liver tissue **(Figure 2A)** to transcriptomic alterations in human liver cancer. For this, we first performed a meta-analysis of human liver cancers (7 transcriptomic datasets with a total of 544 tumor, 260 non-tumor, and 32 healthy patient liver samples) and established which genes were expressed concordantly by cancer and WD-induced alterations in our preclinical mouse model (**Figure S4A,** Suppl Table S3**)**. Among 2080 concordantly expressed genes between WD and cancer, 22% (456 genes), 10% (221 genes) and 3 % (56 genes) were reversed by DHA and EPA, DHA alone and EPA alone, respectively (**Figure 4A left panel,** Suppl Table S4**).** While the current mouse study was designed to assess the effects of ω3 PUFA on preventing NASH, in another study (*41*) we evaluated liver transcriptomes of DHA-treated mice with already established NASH. Preventing pathology is usually easier than to reverse it. Accordingly, we observed that treatment effects of DHA cover ~54% (361 out of 677genes) of its preventive effects relevant for human liver cancer. Hence, these results suggest that DHA can potentially be used as cancer preventive

bioRxiv preprint doi: https://doi.org/10.1101/2022.10.03.510635; this version posted October 5, 2022. The copyright holder for this preprint (which was not certified by peer review) is the author/funder, who has granted bioRxiv a license to display the preprint in perpetuity. It is made available under aCC-BY 4.0 International license.

strategy not only in patients without liver alterations, but also in those with already established NAFLD/NASH (**Figure 4A right panel**).

Next, we asked which of the molecular pathways regulated in cancer and reversed by DHA in mice may mediate the beneficial effects of DHA. For this, we combined gene enrichment analysis with BiBC to focus on genes with the largest impact on cell-cell interactions (see details in M&M). The top enriched pathway was Oxidative Phosphorylation with the well-known pathways such as TGFβ and p53 signaling being enriched to a lesser extent (Figure S4C). One pathway, however, that stood out as highly enriched was the ERBB signaling pathway was also top ranked in mediating DHA-driven cell-cell interactions (i.e., BiBC) (**Figure 4B, Figure S4E**). ERBBs are known homologs of EGFR, which are activated through binding to EGF and related members of the EGF family of growth factors. These include EGF-like ligands or cytokines that are comprised of at least ten proteins including betacellulin, transforming growth factor-alpha (TGF-α), amphiregulin, HB-EGF, epiregulin, and neuregulins and the various other Heregulins (*42-44*).

Using our whole multi-omics network (including DHA affected and not affected genes in NASH) we ranked genes from the ERBB pathway (Figure S4B) based on their potential capacity to mediate effects of DHA and identified betacellulin (BTC), an alternative ligand of EGFR, as a top gene among the important genes (Grb2, Gsk3 Gsk3β/α and Cbl) in the downstream pathway (**Figure 4C**). Interestingly, EGFR itself, although not regulated by DHA was the second best potential regulatory gene for this pathway in NASH. In contrast, BTC was found to be increased in liver cancer meta-analysis (**Figure 4D**), up regulated by WD and downregulated by DHA both in prevention and treatment mouse studies (**Figure 4E**). To ensure the statistical robustness of BTC's potential causal capacity reflected by its high BiBC rankings, we used two additional approaches (non-parametric statistics that would identify outlier values of BiBC and "experimental" statistics by comparing a given node BiBC value to simulated random networks). Each approach demonstrated extremely low probability of BTC being randomly highly ranked (with $p<10^{-15}$ and probability density =0.009, respectively) (**Figure S4D-E**). Thus, we established BTC as a top candidate gene mediating DHA's beneficial effect on hepatic health, while also being relevant for liver cancer in humans.

bioRxiv preprint doi: https://doi.org/10.1101/2022.10.03.510635; this version posted October 5, 2022. The copyright holder for this preprint (which was not certified by peer review) is the author/funder, who has granted bioRxiv a license to display the preprint in perpetuity. It is made available under aCC-BY 4.0 International license.

Figure 4

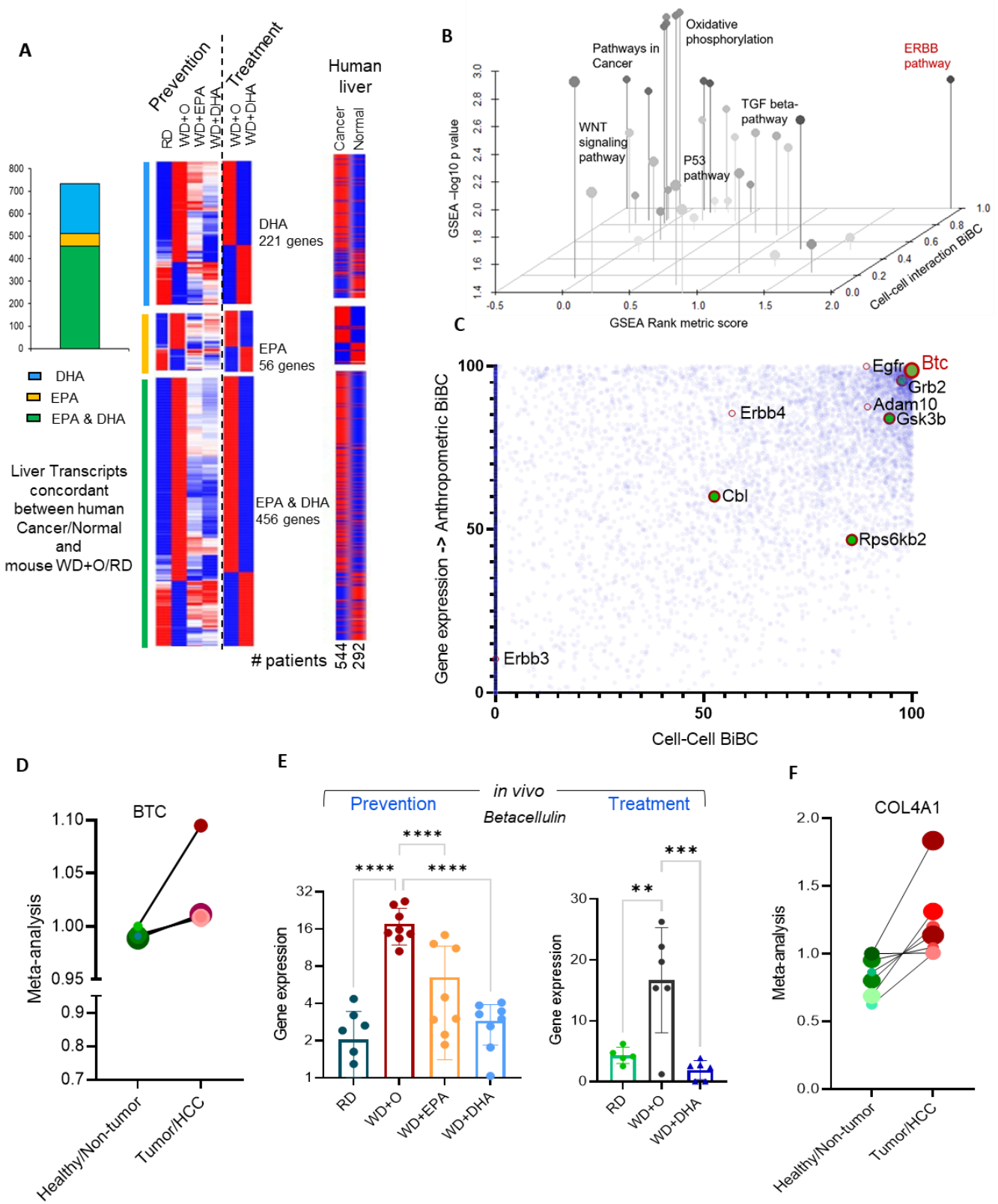

bioRxiv preprint doi: https://doi.org/10.1101/2022.10.03.510635; this version posted October 5, 2022. The copyright holder for this preprint (which was not certified by peer review) is the author/funder, who has granted bioRxiv a license to display the preprint in perpetuity. It is made available under aCC-BY 4.0 International license.

Figure 4. Liver cancer meta-analysis indicates DHA has the potential to prevent NASH to cancer transition

A. The heatmap for genes from human liver cancer meta-analysis (see materials and methods) in the right panel is organized by corresponding genes from mouse study namely, treatment effect determined by analysis of DHA or EPA effects in the prevention study and treatment study, left and center heatmaps. The stacked bar plot shows the distribution of treatment effected genes in prevention study for the genes aligned with human cancer meta-analysis genes.

B. 3D scatter plot showing gene set enrichment analysis (GSEA) Rank score on the x-axis, GSEA -Log10(p-value) on the y-axis, and cell-cell interaction BiBC on the z-axis. Relevant pathways are labeled in the figure (red) with the (BTC)-ERBB pathway ranked highly by all metrics.

C. Scatterplot of NW BiBCs between gene expression and anthropometric parameters plotted against cell-cell BiBCs. Members of the Btc-Erbb pathway genes are overlayed and indicate the importance of Btc-Erbb signaling in the NASH multi-omics network model.

D. BTC gene expression from meta-analysis of human normal and liver cancer datasets indicates a significant increase in liver cancer samples (Effect size FDR = 2.3×10^{-4}). The size of each individual dot represents the number of patients associated with the dataset with higher the number of patients darker the dot color, Normal (green) and Cancer (red) (7 transcriptomic datasets with a total of 544 tumor, 260 non-tumor, and 32 healthy patient liver samples).

E. Bar plot of Btc gene expression in transcriptome of mouse livers from the preventive (n=8/group) and treatment (n=5 or 6/group) experiments. (Data are mean +/- SD, Ordinary One-way ANOVA, multiple comparisons test with WD+O, ns (not significant), *p<0.05, ** p<0.001, *** p<0.005, ****p<0.0001).

F. COL4A1 gene expression from meta-analysis of human normal and liver cancer data indicates a highly significant increase in expression in liver cancer samples (Effect size FDR = 1.37×10^{-13}). The size of each individual dot represents the number of patients associated with the dataset with higher the number of patients darker the dot color, Normal (green) and Cancer (red) (7 transcriptomic datasets with a total of 544 tumor, 260 non-tumor, and 32 healthy patient liver samples).

BTC promotes NASH fibrosis via activating hepatic stellate cells to produce TGFβ-2

Given that BTC was predicted as a new target for effects of DHA in NASH, we next verified which cell types express BTC in our model of NASH. For this, we turned to the single cell RNA-seq data and observed that cholangiocytes (**Figure S5A**) were the primary population of cells expressing BTC. Although its source is restricted to cholangiocytes, BTC's role as a growth factor indicates it can act on many different types of neighboring cells (e.g., hepatocytes, macrophages, hepatic stellate cells and others) that possess EGFR/ERBBs (**Figure S6A**). Among different liver cell types which would respond to BTC and proliferate during NASH progression, hepatic stellate cells (HSCs), frequently called mesenchymal cells in humans (*30*, *45*) producing collagens represent a major contributor to fibrosis. Indeed, the number of mesenchymal cell counts in humans with cirrhosis is markedly higher than those of healthy livers (**Figure S5B**). Importantly, DHA prevents and reverses fibrosis in a NASH mouse model (*12*, *25*) and decreases expression of two out of three collagen encoding genes (COL1A1, COL1A2, COL4A1) that are upregulated in liver cancer (**Figure 4F S5E,** Suppl Table S4). Therefore, we next tested effects

bioRxiv preprint doi: https://doi.org/10.1101/2022.10.03.510635; this version posted October 5, 2022. The copyright holder for this preprint (which was not certified by peer review) is the author/funder, who has granted bioRxiv a license to display the preprint in perpetuity. It is made available under aCC-BY 4.0 International license.

of BTC on human hepatic stellate cells using the LX2 cell line (*46*). LX2 cells were grown and pretreated with and without BTC using EGF as a growth factor positive control(M&M). LX2 growth was significantly increased in a dose-dependent manner by BTC (**Figure 5A**) to a similar extent as was observed for EGF (Figure S5C). Moreover, we observed increased collagen staining (Sirius red) in cells treated with BTC (**Figure 5B**).

We next performed transcriptomic analysis of LX2 cells treated with BTC and compared it to genes regulated by DHA in vivo. We found 63 genes upregulated by BTC and downregulated by DHA and 16 genes downregulated by BTC and upregulated by DHA. Among the enriched pathways for the set of genes induced by BTC and repressed by DHA were involved in cell growth including ERBB signaling (**Figure 5C, Figure S6I,** Suppl Table S5). Strikingly, TGFB2 was the only gene found in common across several enriched categories. Moreover, expression of TGFB2, but not TGFB1 was increased by BTC in vitro (**Figure 5D, S5D),** repressed by DHA in both prevention and treatment mouse studies (**Figure 5E),** and increased in liver cancer meta-analysis (**Figure 5F**). A recent study demonstrated that TGFβ-2, but not TGFβ-1 has a critical non-redundant role in promoting lung and liver fibrosis (*47*). Therefore, we hypothesized that downstream effects of reduction of BTC by DHA can be explained by reduction of TGFβ-2. For this, using publicly available data *in vitro* on TGFβ-2 effects and our *in vivo* data, we evaluated which genes regulated by DHA were regulated in the opposite direction by TGFβ-2. We found 62 genes upregulated by TGFβ-2 and downregulated by DHA and 62 genes downregulated by TGFβ-2 and upregulated by DHA. DHA downregulated/ TGFβ-2-upregulated genes were highly enriched for production of collagen trimers and extracellular matrix organization (**Figure 5G**) while genes downregulated by TGFβ-2 and reversed by DHA were enriched for mitochondrial inner membrane and other mitochondrially related functions (**Figure 5H**). Altogether these results suggest that one of a key mechanism of fibrosis reduction by DHA is achieved through an inhibition of BTC and consequent reduction of HSCs proliferation and TGFβ-2-induced collagen production(*47*).

bioRxiv preprint doi: https://doi.org/10.1101/2022.10.03.510635; this version posted October 5, 2022. The copyright holder for this preprint (which was not certified by peer review) is the author/funder, who has granted bioRxiv a license to display the preprint in perpetuity. It is made available under aCC-BY 4.0 International license.

Figure 5

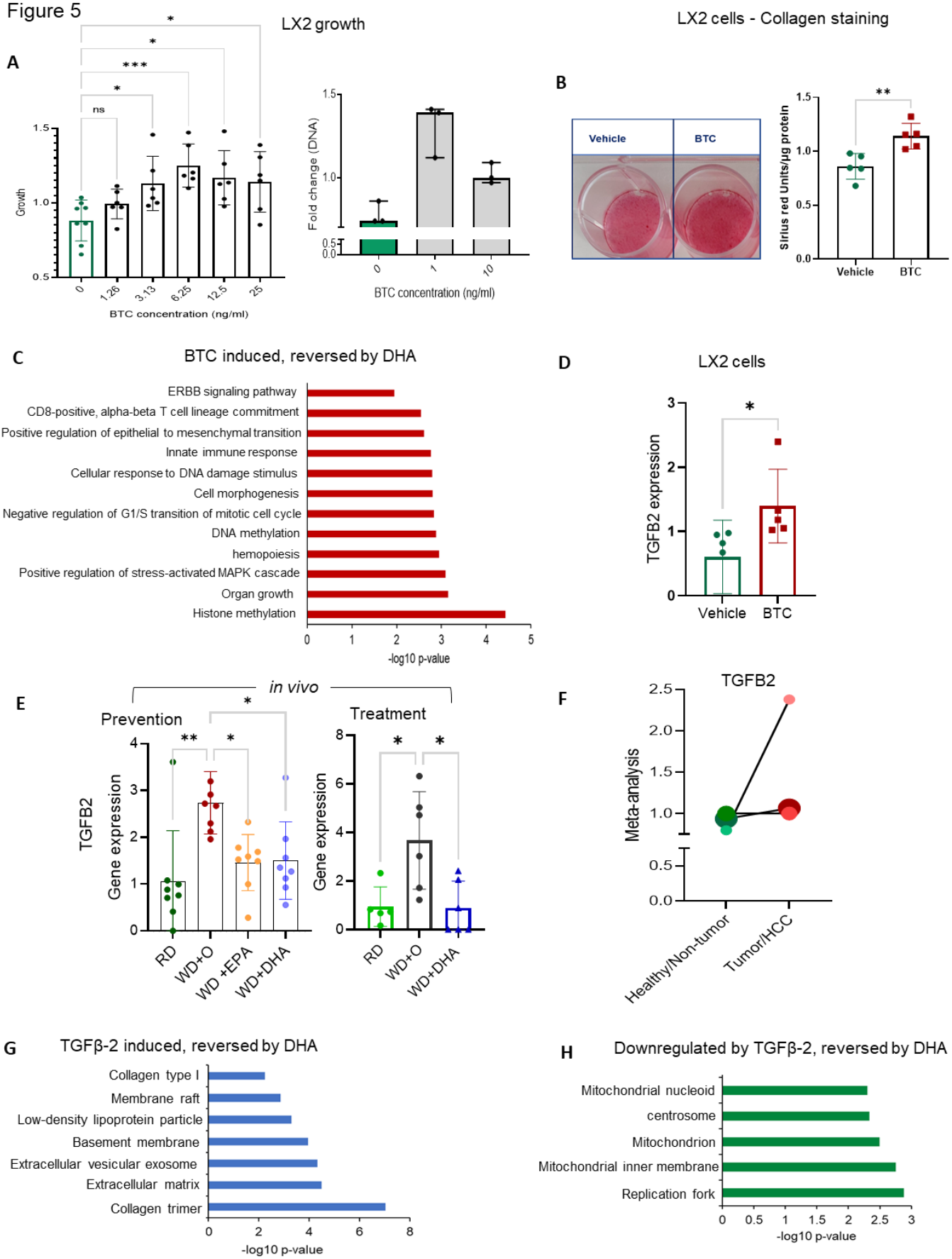

bioRxiv preprint doi: https://doi.org/10.1101/2022.10.03.510635; this version posted October 5, 2022. The copyright holder for this preprint (which was not certified by peer review) is the author/funder, who has granted bioRxiv a license to display the preprint in perpetuity. It is made available under aCC-BY 4.0 International license.

Figure 5. Hepatic stellate cell (LX2) proliferation could promote fibrosis via BTC-TGFβ-2, reversed by DHA

A. LX2 cell proliferation assay after treatment with BTC, 0-25 ng/mL (left panel, n=6 individual experiments). Fold change in DNA concentration after treatment with BTC 0-10 ng/mL (right panel, n=3 individual experiments). Green bar in each plot is untreated control. Data are displayed as mean +/- SD with each point being an individual experiment; Ordinary One-way ANOVA, multiple comparisons test with control vehicle, ns (not significant), *p<0.05, ** p<0.001, *** p<0.005, ****p<0.0001).

B. Collagen staining (Pico Sirius Red, PSR) in LX2 cells indicating increased fibrosis (collagen production) when stimulated with BTC (20mg/ml; 5 separate experiments) or a vehicle control. A representative image of stained cells is shown (left panel). A bar plot of staining intensity normalized by total protein (µg) per well. (N= 5 experiments; unpaired, two-sided t-test **p=0.0058).

C. Gene enrichment (biological process) of LX2 cells (see materials and methods) while induced by BTC (BTC vs Vehicle; one-sided t-test) identifies pathways reversed by DHA treatment *in vivo*. Data are displayed as -log10(p-value).

D. Bar plot of TGFB2 gene expression in LX2 cells treated with vehicle or BTC (20 ng/ml; 5 experiments) *in vitro*; (paired, two-sided t-test *p<0.05, FDR<0.1)

E. TGFB2 expression *in vivo.* DHA reversed the gene expression significantly in the *in vivo* experimental model both in Preventive & Treatment models. Data are displayed as mean_+/- SD, n=6 mice/group (preventative study) or n=4 or 5 mice per group (treatment study); Ordinary One-way ANOVA, multiple comparisons test with control vehicle, ns (not significant), *p<0.05, ** p<0.001, *** p<0.005, ****p<0.0001).

F. The human liver cancer meta-analysis shows the significant increase in TGFB2 in cancer samples. (Effect size FDR <0.0064). The size of each individual dot represents the number of patients associated with the dataset with higher the number of patients darker the dot color, Normal (green) and Cancer (red) (7 transcriptomic datasets with a total of 544 tumor, 260 non-tumor, and 32 healthy patient liver samples).

G. Gene enrichment analysis of genes upregulated in TGFβ-2 treated cells that were reversed by DHA *in vivo* identifies collagen trimer and extracellular matrix as top enriched pathways. Data are displayed as -Log10(p-value).

H. Gene enrichment analysis of downregulated genes in TGFβ-2 treated cells that were reversed by DHA *in vivo* identifies mitochondrial inner membrane and mitochondrion as highly enriched. Data are displayed as -Log10(p-value).

bioRxiv preprint doi: https://doi.org/10.1101/2022.10.03.510635; this version posted October 5, 2022. The copyright holder for this preprint (which was not certified by peer review) is the author/funder, who has granted bioRxiv a license to display the preprint in perpetuity. It is made available under aCC-BY 4.0 International license.

TLR-dependent inflammatory processes in NASH are exacerbated by BTC

Our results from stellate cells support a plausible scenario that inhibition of BTC by DHA would explain reduction of fibrosis and improvement of mitochondrial function. However, reduction in inflammation, another major effect of DHA observed from our initial analyses (Fig. 1 and 2), cannot be interpreted by effects of BTC on stellate cells. Furthermore, we have previously reported that systemic levels of TLR2 ligands are decreased by DHA (**Figure S6B**). These data, along with a well-known fact that a genetic deficiency of microbiota sensors (TLR2 and TLR4) attenuates NASH (*48-50*), indicate that reduction of TLR2 and/or TLR4 ligands by DHA might interact with reduction of BTC in preventing the disease. While different receptors for BTC are widely distributed across different liver cell types (**Figure S6A, S6H**), TLR2 and TLR4 are predominantly expressed by macrophages in the liver (**Figure S6C**). Furthermore, alterations of gene expression related to macrophages by DHA were the top among all cell types detected in the liver (Figure 2B) and EGFR deficiency in macrophages, but not in hepatocytes has been shown to attenuate liver cancer in mouse model (*51*). Taken together, our next question was: which processes regulated by DHA in the liver can be explained by the effects of BTC and TLR2/4 agonists on macrophages? We also asked whether BTC modulates TLR2/4-dependent immune stimulation in macrophages. To answer these questions, we differentiated the human monocyte cell line (THP1) to a macrophage like phenotype and stimulated with BTC, LPS (TLR4 ligand) and PGN (TLR2 ligand) and compared global gene expression in these cells to cells stimulated with TLR2/4 ligands only or unstimulated control cells (**Figure S6I,** Suppl Table S7).

To investigate a potential interaction effect, we tested a range of concentrations of BTC and TLR-agonists evaluating expression of IL-8 and CCL2 (MCP-1) expression, well-known targets of BTC (*51, 52*) and TLR-agonists (*48-50, 53*) and chose the lowest doses that induces their expression (**Figure S6J**). We next performed transcriptomic analysis of THP-1 cells treated with BTC-LPS-PGN and compared it to genes regulated by DHA *in vivo*. We found 179 genes upregulated by BTC-LPS-PGN and downregulated by DHA and 285 genes downregulated by BTC-LPS-PGN and upregulated by DHA (**Figure 6A)**. Genes upregulated by BTC-LPS-PGN were enriched for several pathways related to monocyte/macrophage related immune functions, the cell cycle, and collagen binding. Among the most enriched categories for the downregulated genes were mitochondrion, NAD metabolic process, and endoplasmic reticulum membrane (**Figure 6B-C, S6D-G)**.

To assess the relative contribution of BTC and of TLR2/4 agonists to the observed combined functional effect, we calculated a summary metric for each pathway (see M&M) and compared their values between each treatment group (**Figure 6D)**.

To check if the expected effects of BTC are present in macrophages, we first verified expression of EGFR/cell cycle and EMT pathways and observed their increase among the categories upregulated by BTC alone and in combination with TLR agonists (**Figure 6E)**. Analysis of the downregulated pathways showed that in combination with TLR ligands BTC inhibited expression of genes involved in mitochondrial functions (TCA cycle, oxidative

bioRxiv preprint doi: https://doi.org/10.1101/2022.10.03.510635; this version posted October 5, 2022. The copyright holder for this preprint (which was not certified by peer review) is the author/funder, who has granted bioRxiv a license to display the preprint in perpetuity. It is made available under aCC-BY 4.0 International license.

phosphorylation, **Figure S6G**) and NAD metabolic functions (critical pathways operating in mitochondria (*54-56*) (**Figure 6F**).

As for the upregulated pathways, we observed diverse immune functions such as 'innate immune response', 'regulation of interferon-gamma signaling' with a similar or slightly enhanced expression of genes when BTC was added with TLR2/4 agonists (**Figure 6G, Figure S6F**). However, some genes showed clear interactions between BTC and TLR-agonists. For example, IL1B was upregulated by TLR2/4 agonists and slightly increased by BTC, but CSF1, a classical factor of macrophage growth and proliferation (*57*), was upregulated only when both BTC and TLR2/4- agonists were present (**Figure 6H**).

Among immune related pathways, the strongest BTC effect either alone or in combination with TLR2/4 agonists was on the integrin-mediated signaling pathway, which partially overlapped with collagen binding (**Figure 6I**). Interestingly, while there was a trend of an effect of BTC ITGα6 and ITGα9 and TLR2/4 agonists on ITGα1, only combination of BTC with TLR-agonists significantly induced expression of all three integrins (**Figure 6J, S6D**).
Notably, the integrin pathway was not regulated by TLR2/4 agonists alone suggesting a possible unique role of the crosstalk between EGFR and TLR pathways in controlling fibrosis related molecular function in macrophages **(Figure 7).**

Figure 6. BTC promotes TLR-dependent inflammation and integrin production by macrophage (THP1) cells

A. Differential expression with BTC-LPS-PGN treated cells to control THP-1 cells (p-value<0.05) against in vivo differential expression with WDO to WD+DHA. Scatterplot of differentially expressed genes *in vitro* (BTC-LPS-PGN/control in THP-1 cells; p-value <0.05) plotted against expression *in vivo* (WD+DHA/WD+O fed mice). Filled circles are the genes in DHA treatment category.
B. Innate immune response, cell cycle, integrin-mediated signaling pathway, and collagen binding function are enriched (Gene ontology-biological process) by BTC-LPS-PGN treatment in THP-1 cells. Data are displayed as -log10(p-value).
C. The mitochondrion and related functions as well as NAD metabolic process (Gene ontology-biological process and cellular components) are significantly down regulated in BTC-LPS-PGN treated THP-1 cells. Data are displayed as -log10(p-value).
D. Summary metric of all major molecular pathways affected by BTC treatment in THP-1 cells shown to be prevented by DHA in both *in vivo* preventive and treatment models.
E-H. The individual pathways enriched in BTC-LPS-PGN treated THP-1 cells but reversed by DHA *in vivo* in the NASH preventive and treatment models displayed as summary metric (see materials and methods). Individual gene expression IL-1b and CSF1 *in vivo* and THP-1 cells *in vitro*.
I-J. The integrin signaling and collagen pathway summary metric are shown. ITGA1 is shown in THP1 cells treated with BTC-LPS-PGN and vivo NASH preventive model.

bioRxiv preprint doi: https://doi.org/10.1101/2022.10.03.510635; this version posted October 5, 2022. The copyright holder for this preprint (which was not certified by peer review) is the author/funder, who has granted bioRxiv a license to display the preprint in perpetuity. It is made available under aCC-BY 4.0 International license.

Figure 6

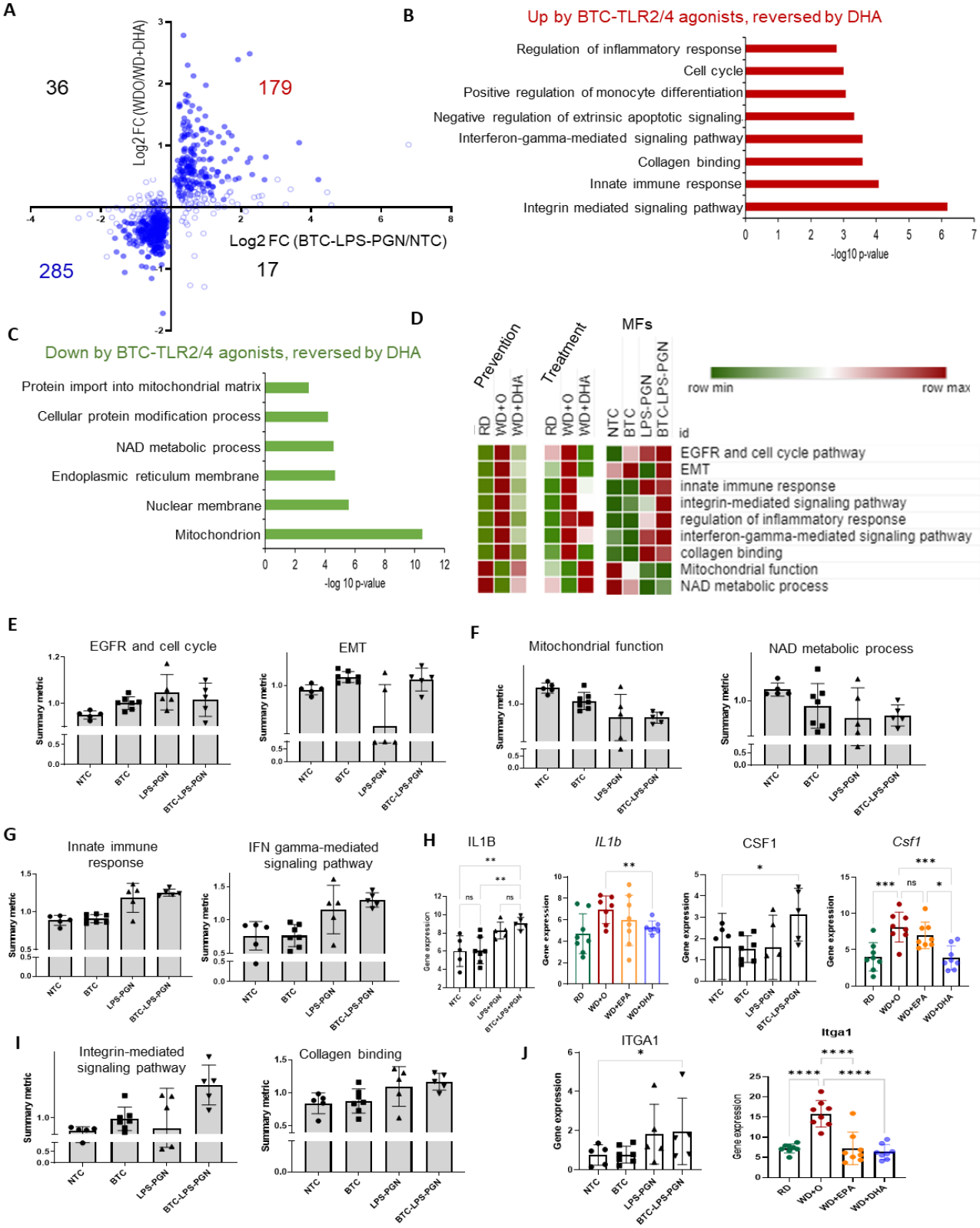

bioRxiv preprint doi: https://doi.org/10.1101/2022.10.03.510635; this version posted October 5, 2022. The copyright holder for this preprint (which was not certified by peer review) is the author/funder, who has granted bioRxiv a license to display the preprint in perpetuity. It is made available under aCC-BY 4.0 International license.

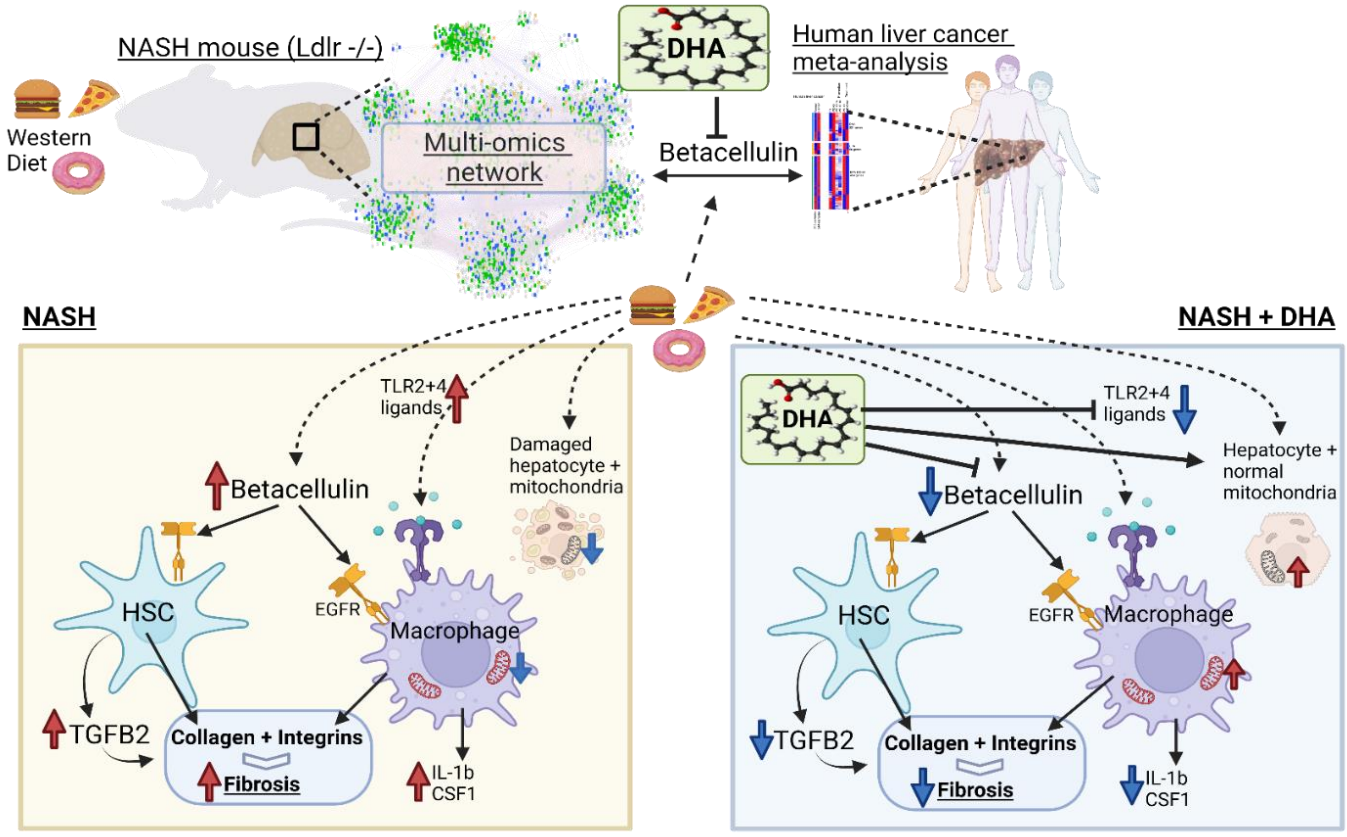

Figure 7. Proposed pathway for the DHA attenuation of BTC effects on liver.
Based on mouse and human single cell RNASeq studies, BTC is expressed in cholangiocytes and acts locally to regulate the ERBB pathway in various liver cells, e.g., hepatic stellate cells (HSC) and macrophages (MFs). NASH is associated with increased BTC expression in human and mouse livers. DHA inhibits BTC expression in livers of mice fed the western diet. BTC effects on LX2 cells (HSC) include increased cell proliferation and TGFβ-2 expression leading to collagen production, while BTC effects on THP-1 cells (MFs) involves increased production of key cytokines and integrins. DHA blocks these pathways by inhibiting the BTC's action on these cells lead to decreased fibrosis, hepatic inflammation and improves mitochondrial function as seen in vivo.

bioRxiv preprint doi: https://doi.org/10.1101/2022.10.03.510635; this version posted October 5, 2022. The copyright holder for this preprint (which was not certified by peer review) is the author/funder, who has granted bioRxiv a license to display the preprint in perpetuity. It is made available under aCC-BY 4.0 International license.

Discussion

For the majority of illnesses which together constitute metabolic diseases such as diabetes (*58, 59*), atherosclerosis (*60*), and obesity (*61*) there are highly efficient drugs that treat and/or prevent development of these diseases. The only frequent representative of metabolic diseases that still lacks pharmacological agents that would pass clinical trials is NAFLD/NASH. As this disease is often called "fatty liver", most of attempted treatments target reduction of liver fat (*62*). However, these treatments cannot resolve liver fibrosis, which seems to be a much more resistant aspect of the pathogenesis of this disease (*63*). Fibrosis is the main cause of liver failure in patients with NASH and also precedes and leads to development of liver cancer (*8, 64*). Therefore, revealing the mechanisms of action of DHA that reduce fibrosis in a preclinical mouse model may aid in the intelligent use of ω3 PUFA or help in developing new drugs that would act upon the same cellular/molecular targets (*5*).

In this study, we identified betacellulin (BTC), one of the alternative ligands of EGFR, as a master regulator whose reduction by DHA potentially leads to prevention/treatment of fibrosis. Indeed, we revealed that BTC induces the TGFβ-2, a critical contributor to liver fibrosis via collagen production by hepatic stellate cells (*65*). Moreover, in combination with TLR 2/4-agonists (also reduced by DHA), BTC induces integrin pathway in macrophages, the cell type in the liver most affected by DHA treatment and well-known to be involved in pathogenesis of fibrosis in different organs (*66*) (Figure 2B, 7).

In addition to its effect on fibrosis, reduction of BTC seems to be also mediating another important effect of DHA which is improvement of mitochondrial function related pathways. Indeed, mitochondrial damage is widely reported in NAFLD/NASH and its improvement by DHA is clearly seen even at the initial stage of our analysis (Figure 1E) indicating strong impact of DHA on this pathway. Accordingly, the integrative network analysis revealed that a restoration of lipids that make up the mitochondrial membrane (sphingomyelins) and precursors of cardiolipin together with Lpgat1 and Taz were at the center of lipidomic-transcriptomic interaction restored by DHA (*36-38*). Noteworthy, mitochondrial dysfunction due to LPGAT1 defects are known to play a major role in metabolic diseases, development of NAFLD and hepatic insulin resistance in obese patients (*67*). While several probiotic microbes have been shown to reverse liver mitochondrial damage(*68, 69*), BTC in combination with microbiota derived stimulation (represented by Tlr-agonists) has a negative effect on the expression of genes involved in mitochondrial functions. Intriguingly, combination of these stimuli (BTC+TLR-agonists) did not affect expression of genes directly involved in the cardiolipin pathway except one (TAMM41) in HSCs. This may be related to the fact that the cardiolipin pathway genes are primarily expressed in hepatocytes, a cell type that was not tested in our study.

Another strong effect of DHA observed at the initial step of our analysis was inhibition of inflammation (Figure 1E). Not surprisingly, a deeper investigation into this phenomenon led us to potential effects of DHA on microbiota-related molecules and a specific sub-type of immune cells in the liver involved in sensing microbes. In fact, network analysis combined with scRNAseq data pointed to macrophages as main cellular targets of DHA in the liver (Figure 2B).

bioRxiv preprint doi: https://doi.org/10.1101/2022.10.03.510635; this version posted October 5, 2022. The copyright holder for this preprint (which was not certified by peer review) is the author/funder, who has granted bioRxiv a license to display the preprint in perpetuity. It is made available under aCC-BY 4.0 International license.

Macrophages are also the primary cells in the liver that express both TLR 2/4 (Figure S6C) whose microbiota-derived agonists are decreased by DHA (Figure S6B)(*25*). This was an important observation considering that deficiency of either TLR2 or TLR4 attenuates severity of NADFL/NASH in mouse models (*48-50*).

In contrast to TLRs, EGFR and other receptors that BTC binds are widely expressed across most cells in liver including macrophages. Thus, it is plausible that the impact of DHA on macrophage related to NAFLD/NASH pathogenesis can be explained by the fact that DHA simultaneously limits cell access to BTC and TLR2/4 agonists. Interestingly, despite the limitations of our cell culture system and the difficulty of transition from mice to humans, we observed that BTC combined with TLR 2/4 agonists induce the integrin signaling pathway which was inhibited by DHA in the liver. Inspecting individual genes revealed that all detected integrins (ITGα1,6,9- Figure 6J, Figure S6D) required all three compounds for induction except for ITGβ1 that increased only with only BTC stimulation in THP-1 cells. Interestingly, ITGβ1 was also increased by BTC in hepatic stellate cells (Figure S5G). Of note, proteins coded to ITGαs and ITGβs form a complex that binds collagens (*70*). Accordingly, blocking integrin signals has been shown to attenuate fibrosis (*71, 72*). Hence, our results taken together with already existing literature about other pathologies (*70*) suggest that DHA inhibits the macrophage contribution to fibrosis by simultaneously inhibiting microbiota-derived signals and BTC. Furthermore, while BTC is a new player in this arena, the role of microbiota derived signals in activating a profibrotic program in macrophages has been reported for different diseases in a few organs (*73, 74*).

Leveraging complex multi-omics and single cell data while using a systems approach, our study constructed a statistical network model of cell-cell interactions affected by DHA (Figure S2B). More importantly, network cause-effect related information flow (degree and BiBC) combined with a ligand-receptor database (Figure S2E) allowed us to infer that a candidate master regulator molecule (BTC) produced by one cell (cholagiocytes) acts upon several other cells. DHA may affect several cell types involved in liver fibrosis. Our study, however, reveals that BTC inhibition by DHA simultaneously disrupts of the integrin pathway in macrophages and TGFβ-2 -driven collagen production by hepatic stellate cells, two processes that synergize in the development of liver fibrosis. Thus, we propose that removal of BTC and Tlr2/4 agonists prevents binding of integrins to collagen that is required for full scar development.

The main outcomes of our study, however, might miss some beneficial effects of DHA, especially those that are not related to BTC reduction and fibrosis. This is because we focused our investigations on cellular/molecular events relevant to liver cancer in humans. Specifically, while our network analysis modeled NASH in mice, we used it as a first step in identification of the most critical causal pathways upregulated in hepatic cancer meta-analysis and reversed by DHA. In this analysis we found ERBB as a top pathway with BTC being the top-ranked molecule in this pathway altered by DHA. Accordingly, our *in vitro* investigations of hepatic stellate cells demonstrated that BTC promotes cell growth, which was an expected finding

bioRxiv preprint doi: https://doi.org/10.1101/2022.10.03.510635; this version posted October 5, 2022. The copyright holder for this preprint (which was not certified by peer review) is the author/funder, who has granted bioRxiv a license to display the preprint in perpetuity. It is made available under aCC-BY 4.0 International license.

considering that BTC belongs to a family of growth factors (*42-44*). Our gene expression analyses of effects promoted by BTC *in vitro* and downregulated by DHA in the liver also support this growth function for BTC (Figure 5A), pointing to an activation of ERBB pathways, cell growth and even the epithelial mesenchymal transition. Dysregulation of these pathways are hallmarks of cancer (*51, 75, 76*). The growth-promoting actions of BTC are known to be mediated by epidermal growth factor receptors (ERBBs), namely ERBB1(EGFR) (*75*), ERBB2, ERBB3 and ERBB4. In liver however, the mechanism for BTC dependent cell proliferation has not been elucidated. The BTC-EGFR-ERBB4 pathway in pancreatic ductal adenocarcinoma has been well established by several groups and a BTC knock out can partially rescue the cancer progression (*77*). In the *in vivo* NASH model, we have a significant reversal of ERBB4 expression by DHA (Figure S6H). Furthermore, DHA also inhibits GRB2 and GSK3β, genes which are downstream in the ERBB signaling pathway found in our liver cancer meta-analysis (Figure 4A, C) and known to promote multiple types of cancers (*74*). These results suggests that DHA, besides its main effect as BTC reduction, might also inhibit residual activation of ERBB pathway via BTC-unrelated mechanisms. In addition, forty-nine EMT related genes, including the TGFβ-2 mediated (*65*) SMAD-EMT-cancer pathway were reversed by DHA treatments (Figure 4A). Therefore, our results suggest that the DHA attenuation of BTC-TGFβ-2 -dependent molecular events might not be limited to reversal of fibrosis in NASH (*25*) but also has a promise in preventing NASH's progression into liver cancer.

Clinical trials using EPA and/or DHA in NAFLD/NASH therapy have shown mixed, but promising results with significant improvement with disease severity, including hepatosteatosis and liver injury (*19-24*). Unfortunately, these studies did not address whether patients that did not respond to therapy represent a cellular/molecular subtype of NAFLD that is not treatable only by ω3 PUFA or perhaps have such severe disease that they are unlikely to respond to any therapeutic agent.

In conclusion, with the discovery of BTC as one of key mediators of ω3 PUFA therapeutic effects, our study opens a new avenue for investigation of NAFLD/NASH. In addition to finding new mechanisms of action of DHA, this study is the first to demonstrate that BTC can induce TGFβ-2 and synergize with microbial signals in the induction of integrins. Thus, while few earlier studies (*78*) showed increase of BTC in the liver tumors, our robust meta-analysis coupled with evidence for causal contributions shed a new light to this molecule in the pathogenesis of this cancer. Moreover, BTC's role in human NAFLD/NASH is entirely uncharted territory. Therefore, future studies should investigate if BTC-triggered gene expression signatures can serve as biomarkers guiding personalized ω3 PUFA therapy, as targets of new NAFLD/NASH drugs, and finally as a predictors of hepatic cancer risk in humans.

bioRxiv preprint doi: https://doi.org/10.1101/2022.10.03.510635; this version posted October 5, 2022. The copyright holder for this preprint (which was not certified by peer review) is the author/funder, who has granted bioRxiv a license to display the preprint in perpetuity. It is made available under aCC-BY 4.0 International license.

Acknowledgments:

We would like to thank Dr. Scott Friedman from the Division of Liver Diseases at the Icahn School of Medicine at Mount Sinai for providing the LX2 cell line and the personnel of CQLS at the Oregon State University for IT support.

Funding:

US Department of Agriculture, National Institute of food and agriculture grant 2009-65200-05846 (DBJ), National Institutes of Health grants, R01 DK094600 (DBJ), R01 DK112360 (DBJ) and R01 DK103761 (NS).

Author contributions

Conceptualization: JP, NN, MGJ, JP, AM, NS, DBJ Methodology: JP, NN, SS, PM, MGJ, JP, RR, ZL, AKD, KB, AM, NS, DBJ Investigation: JP, NN, MGJ, JP, PM, RR, ZL, AKD, KB, GT, AM, NS, DBJ Visualization: JP, NN, JP, AM, NS, DBJ Funding acquisition: AM, NS, DBJ, GT Project administration: NS, DBJ, AM Supervision: AM, NS, DBJ Writing – original draft: JP, NN, NS, AM, DBJ Writing – review & editing: JP, NN, MGJ, JP, SS, RR, ZL, AKD, GT, KB, NS, DBJ, AM

Competing interests: Authors declare that they have no competing interests

Data and materials availability

Sequencing data are deposited in under accession numbers GSE

The complete metabolomic dataset can be accessed here https://www.ebi.ac.uk/metabolights/MTBLS6001.

Supplementary Materials:

Fig. S1 to **Fig. S6** for multiple supplementary figures with the legends.
Table S1. The table shows all differentially expressed genes (DEGs), parameters between WD and ND in mice (FDR<10%) and DEGs that were retained in the network from the liver NASH prevention and treatment study model and their cell type assignments.

Table S2. The data for cardiolipin network model related genes and lipids.

Table S3. Human liver cancer datasets and sample details used in meta-analysis.

Table S4. Meta-analysis of human liver cancer data.

Table S5. Gene expression from LX2 cells with or without BTC treatment mapped on to the NASH network genes.

Table S6. Gene expression from TGFβ-2 treatment mapped on to NASH network genes.

Table S7. Gene expression from THP-1 cells with or without BTC and LPS/PGN treatment mapped on to the NASH network genes.

bioRxiv preprint doi: https://doi.org/10.1101/2022.10.03.510635; this version posted October 5, 2022. The copyright holder for this preprint (which was not certified by peer review) is the author/funder, who has granted bioRxiv a license to display the preprint in perpetuity. It is made available under aCC-BY 4.0 International license.

Supplementary Figures

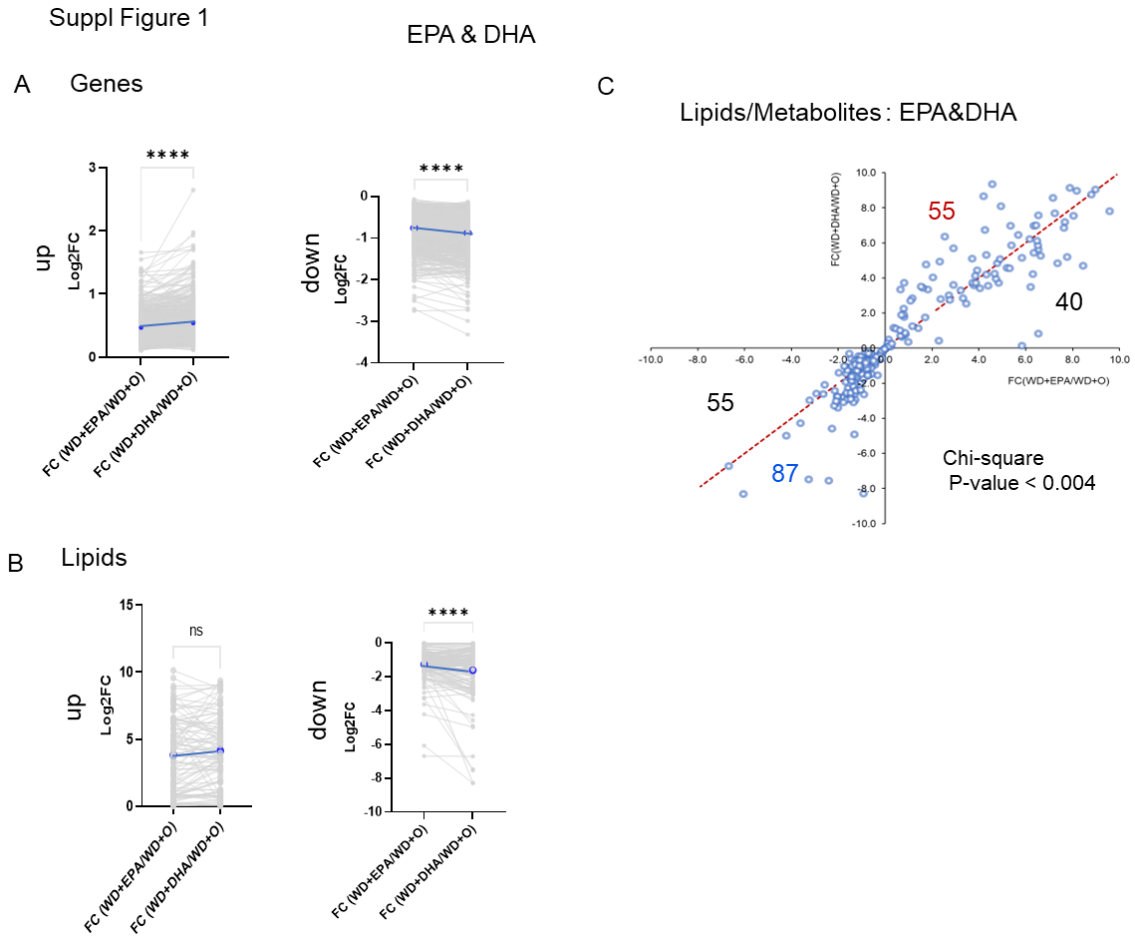

Suppl Figure 1. A-C. The Log2FC of EPA & DHA gene expression (A) and lipids and metabolites (B-C) shows the extent of DHA reversal effects as significantly higher than EPA though similar in profile.

bioRxiv preprint doi: https://doi.org/10.1101/2022.10.03.510635; this version posted October 5, 2022. The copyright holder for this preprint (which was not certified by peer review) is the author/funder, who has granted bioRxiv a license to display the preprint in perpetuity. It is made available under aCC-BY 4.0 International license.

Suppl Figure 2

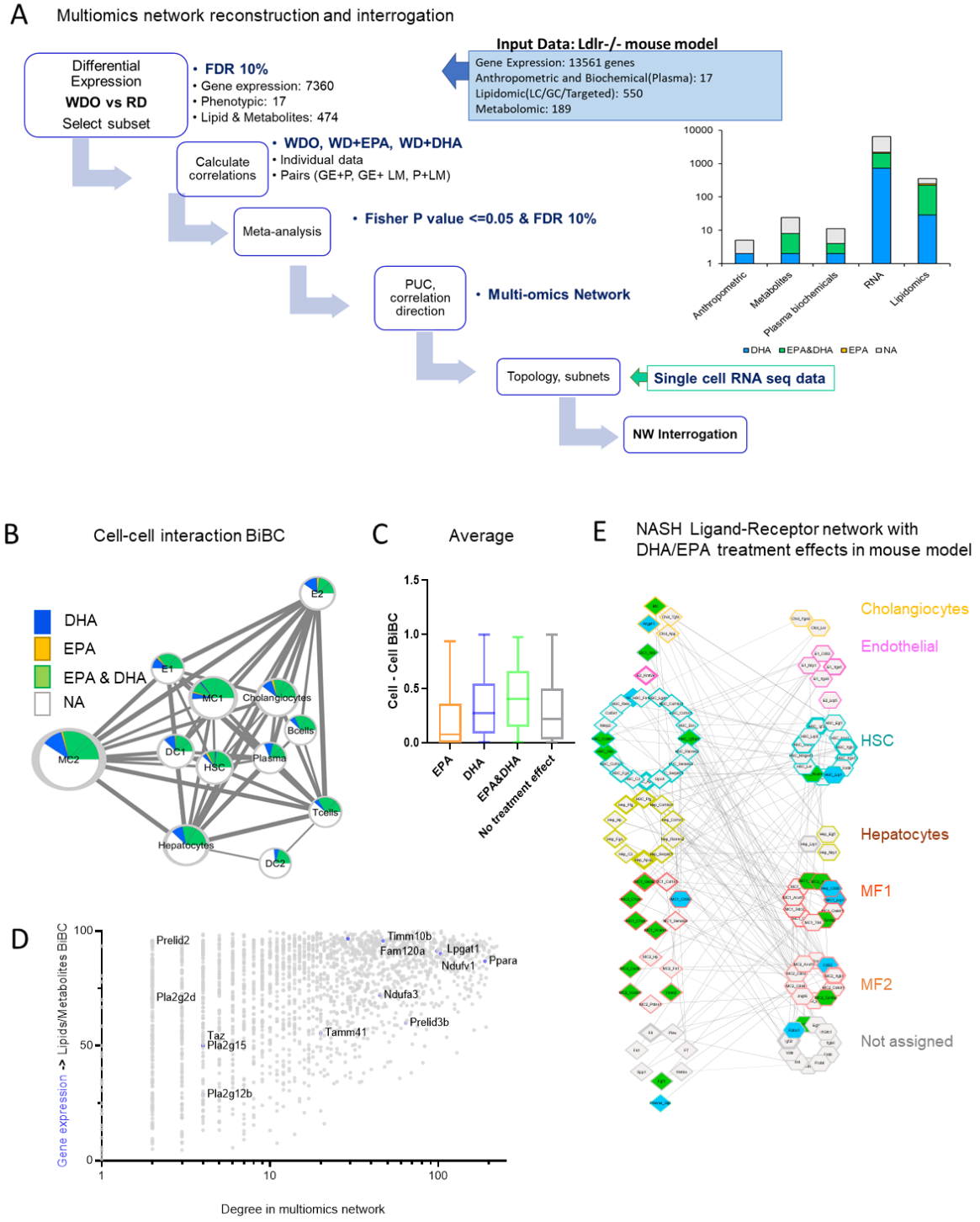

Suppl Figure 2. A. An outline to derive and analyze network model from the multi-omics NASH data. The distribution of treatment effects in the network parameters is shown in the right panel.
B. Outline of cell-cell interactions used to calculate the interaction BiBCs.
C. Box plot of Average cell-cell interaction BiBC for the genes belonging to each treatment effect category (DHA (blue), EPA&DHA (green), EPA (orange) and no category (grey). From the network cell-cell BiBC analysis, genes

bioRxiv preprint doi: https://doi.org/10.1101/2022.10.03.510635; this version posted October 5, 2022. The copyright holder for this preprint (which was not certified by peer review) is the author/funder, who has granted bioRxiv a license to display the preprint in perpetuity. It is made available under aCC-BY 4.0 International license.

regulated by DHA, DHA&EPA have higher median BiBC which indicates a higher causal contribution to cell-cell communication than genes regulated by EPA.
D. The scatterplot indicates the network gene expression and lipids/Metabolites BiBC verses degree. The genes important for lipid metabolism and mitochondrial cardiolipin pathway are labeled.
E. NASH Ligand-Receptor network with DHA/EPA treatment effects in NASH mouse model. The individual cells expressing the genes inferred from single cell RNA sequence reanalysis are overlayed and cell specific interactions are interrogated. Nodes are shown as diamonds (ligands), or hexagon (receptors) and edges are the correlation between the nodes. Node color is according to the treatment effect. The thickness of the nodes is the cell-cell interaction BiBC, higher the better and is shown as thicker. Each cell type and their respective genes are colored differently as labeled.

bioRxiv preprint doi: https://doi.org/10.1101/2022.10.03.510635; this version posted October 5, 2022. The copyright holder for this preprint (which was not certified by peer review) is the author/funder, who has granted bioRxiv a license to display the preprint in perpetuity. It is made available under aCC-BY 4.0 International license.

Suppl Figure 3

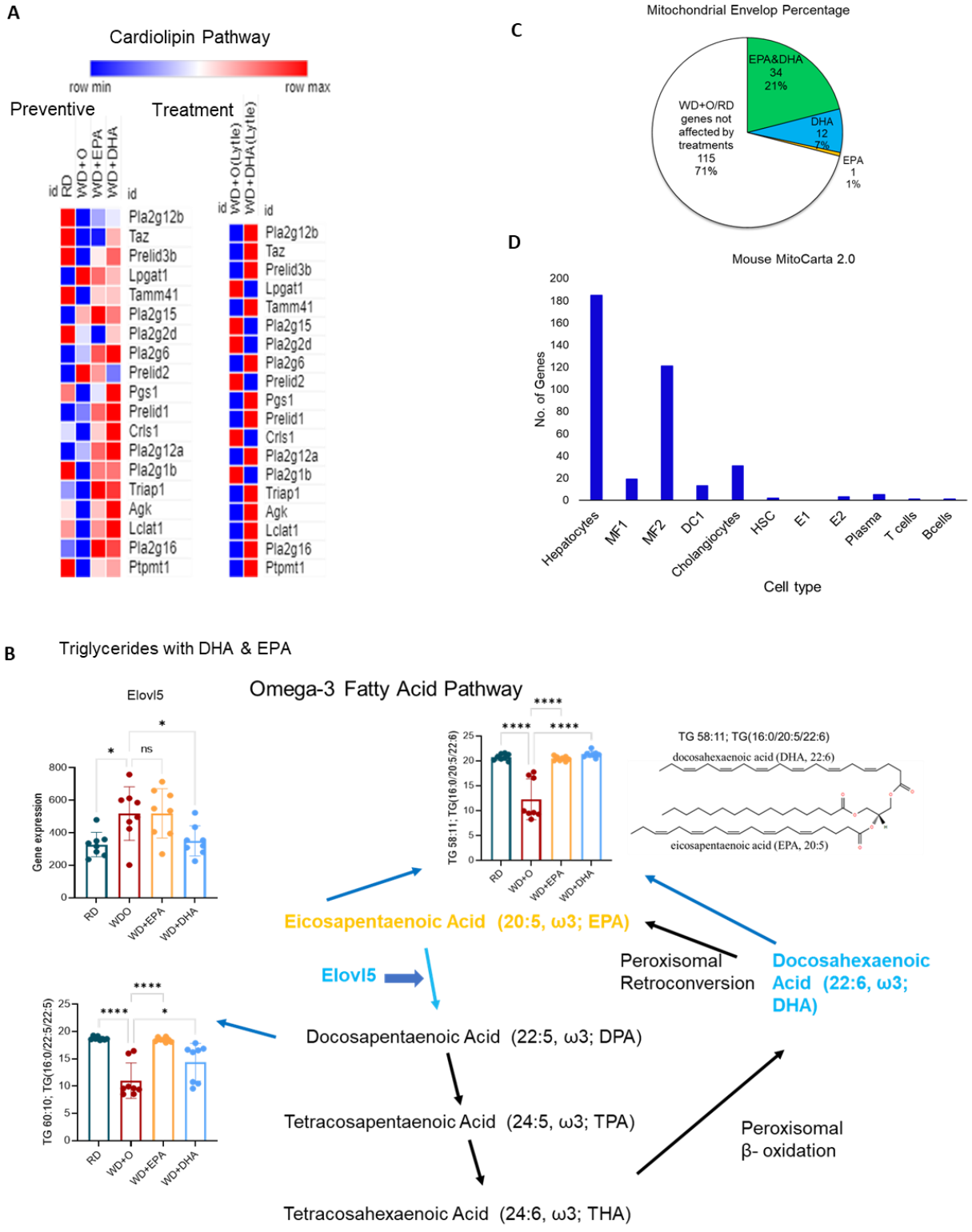

bioRxiv preprint doi: https://doi.org/10.1101/2022.10.03.510635; this version posted October 5, 2022. The copyright holder for this preprint (which was not certified by peer review) is the author/funder, who has granted bioRxiv a license to display the preprint in perpetuity. It is made available under aCC-BY 4.0 International license.

Suppl Figure 3. A. Cardiolipin pathway gene expression with preventive and treatment models. The color scale is indicated from high expression of the genes in red to low in blue.
B. The ω3 fatty acid pathway with peroxisomal retro-conversion and β-oxidation involving Elovl5 and the EPA, DHA conversion steps and intermediates are shown. The TG containing both EPA and DHA in the top BiBC is show as an example of the ω3 fatty acid storage compound.
C. The pie chart for treatment effect on mitochondrial envelop genes in NASH network as annotated using mouse MitoCarta 2.0 database. Colors indicate percent treatment effects as labeled.
D. The cell type distribution for the mitochondrial genes

bioRxiv preprint doi: https://doi.org/10.1101/2022.10.03.510635; this version posted October 5, 2022. The copyright holder for this preprint (which was not certified by peer review) is the author/funder, who has granted bioRxiv a license to display the preprint in perpetuity. It is made available under aCC-BY 4.0 International license.

Suppl fig 4.

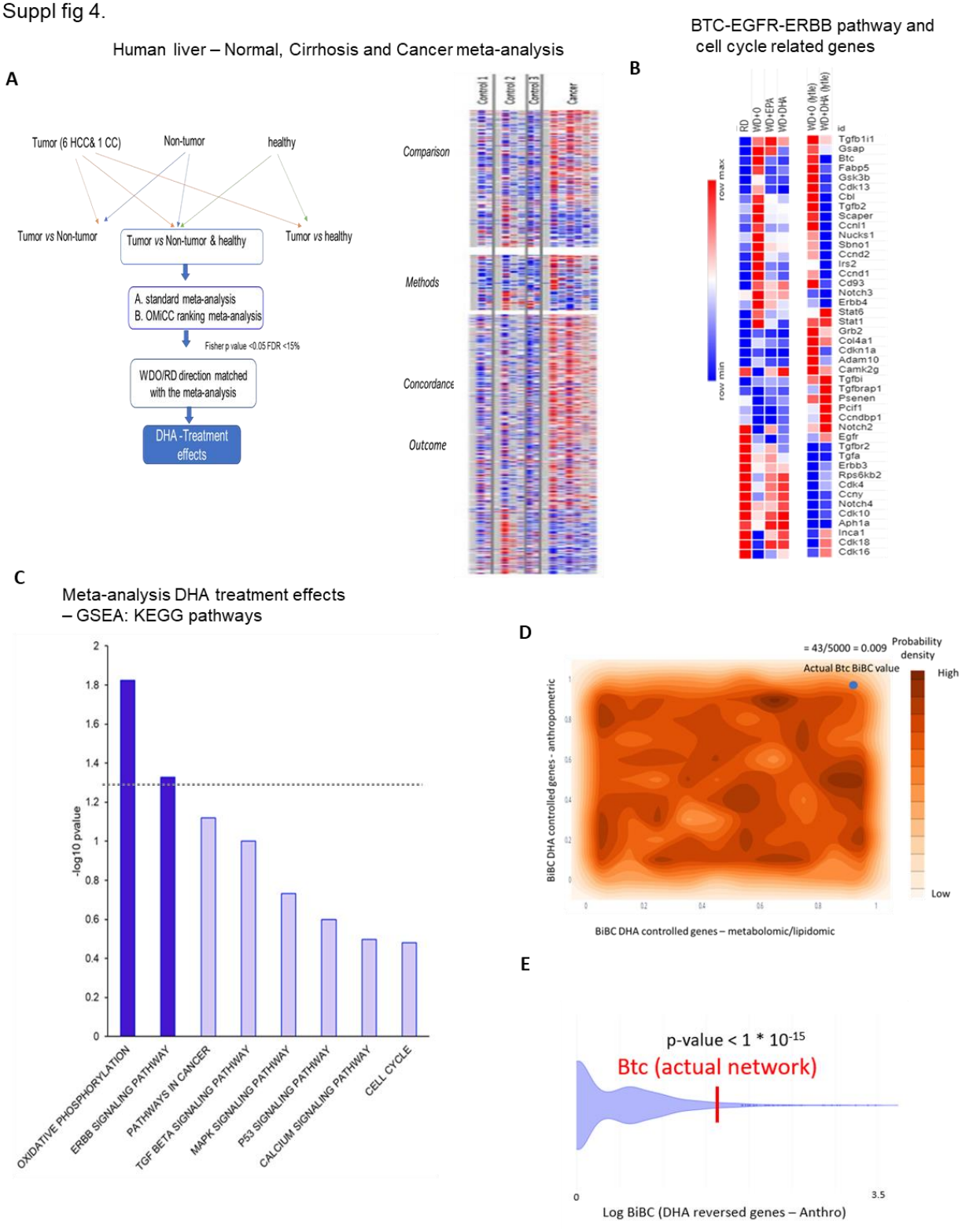

bioRxiv preprint doi: https://doi.org/10.1101/2022.10.03.510635; this version posted October 5, 2022. The copyright holder for this preprint (which was not certified by peer review) is the author/funder, who has granted bioRxiv a license to display the preprint in perpetuity. It is made available under aCC-BY 4.0 International license.

Suppl Figure 4. A. Outline for human liver cancer meta-analysis for the orthologous genes representing the NASH mouse model. Right panel shows the heatmap of mapped genes with treatment effects from individual datasets
B. The gene expression for BTC-EGFR-ERBB pathway and cell cycle related genes in the NASH mouse preventive and treatment models. The color scale is indicated from high expression of the genes in red to low in blue.
C. The bar graph of gene set enrichment analysis using GSEA (KEGG pathways) for the human cancer meta-analysis genes with DHA treatment effects in mouse model. Data are displayed as -Log10(p-value).
D. Distribution of Btc BiBC values calculated between DHA controlled genes and metabolomic/lipidomic data (x-axis) and DHA controlled genes and anthropometric data (y-axis) in 5000 random networks. Dark regions represent areas where a calculated Btc BiBC value is more likely to be found due to random chance. The probability of finding an actual Btc BiBC value equal to or higher than those seen in the random networks (43/5000) is 0.009.
E. Violin plot of the BiBC of Btc between DHA reversed genes and anthropometric data in 5,000 random networks compared to its actual BiBC value in the reconstructed network (one sample Wilcoxon test $p < 1 * 10^{-15}$).

bioRxiv preprint doi: https://doi.org/10.1101/2022.10.03.510635; this version posted October 5, 2022. The copyright holder for this preprint (which was not certified by peer review) is the author/funder, who has granted bioRxiv a license to display the preprint in perpetuity. It is made available under aCC-BY 4.0 International license.

Suppl Fig 5

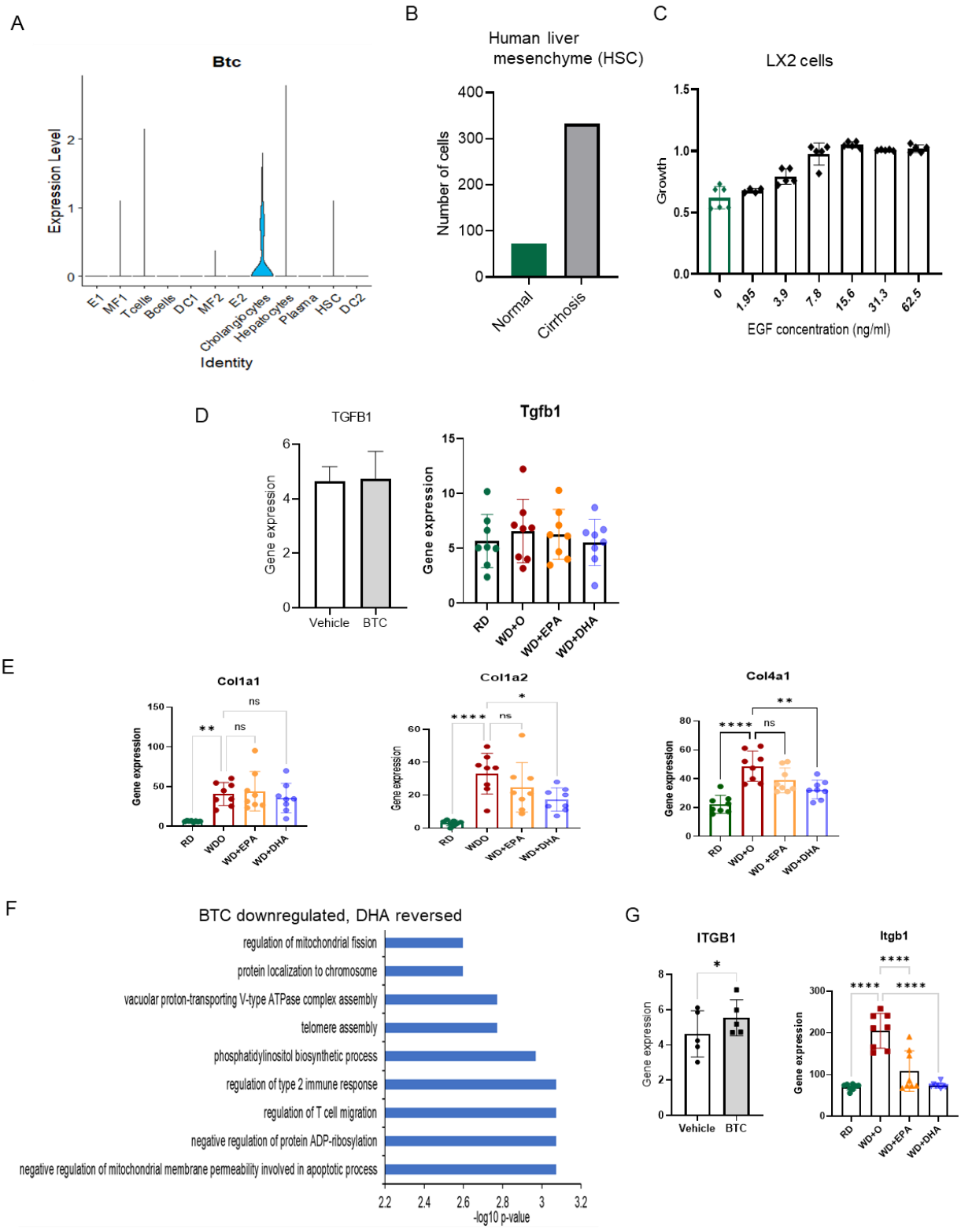

bioRxiv preprint doi: https://doi.org/10.1101/2022.10.03.510635; this version posted October 5, 2022. The copyright holder for this preprint (which was not certified by peer review) is the author/funder, who has granted bioRxiv a license to display the preprint in perpetuity. It is made available under aCC-BY 4.0 International license.

Suppl Figure 5. A. The expression of Btc in Mouse NASH liver single cell RNA sequence data shown here with the maximum expression in liver cholangiocytes.
B. The number of Mesenchymal cells (Hepatic stellate cells) in Human liver samples with enrichment in Cirrhosis with more than 3-fold increase in numbers than normal liver samples.
C. The growth of LX2 cells in response to EGF in a dose dependent manner shown in the bar graph.
D. TGFβ-1 expression in LX2 cells treated with BTC (grey) (20 ng/ml; 5 separate experiments, paired, one-sided t-test, ns (not significant), *p<0.05) and in the NASH preventive model is shown in bar graphs colored by treatment effects (Ordinary One-way ANOVA, with multiple comparisons test with WD+O, ns (not significant), *p<0.05, ** p<0.001, *** p<0.005, ****p<0.0001).
E. The different collagen gene expression in the NASH preventive model shown in bar graphs colored by treatment effects (Ordinary One-way ANOVA, with multiple comparisons test with WD+O, ns (not significant), *p<0.05, ** p<0.001, *** p<0.005, ****p<0.0001).
F. The gene enrichment analysis indicates that regulation of mitochondrial fission and mitochondrial membrane permeability mediated apoptotic pathway are significantly down regulated by BTC treatment in LX2 cells while they are reversed by DHA treatment in the *in vivo* mouse model.
G. ITGB1 expression in LX2 cells treated with BTC (grey) (20 ng/ml; 5 separate experiments, paired, one-sided t-test, ns (not significant), *p<0.05) and in the NASH preventive model is shown in bar graphs colored by treatment effects (Ordinary One-way ANOVA, with multiple comparisons test with WD+O, ns (not significant), *p<0.05, ** p<0.001, *** p<0.005, ****p<0.0001).

bioRxiv preprint doi: https://doi.org/10.1101/2022.10.03.510635; this version posted October 5, 2022. The copyright holder for this preprint (which was not certified by peer review) is the author/funder, who has granted bioRxiv a license to display the preprint in perpetuity. It is made available under aCC-BY 4.0 International license.

Figure 6 suppl

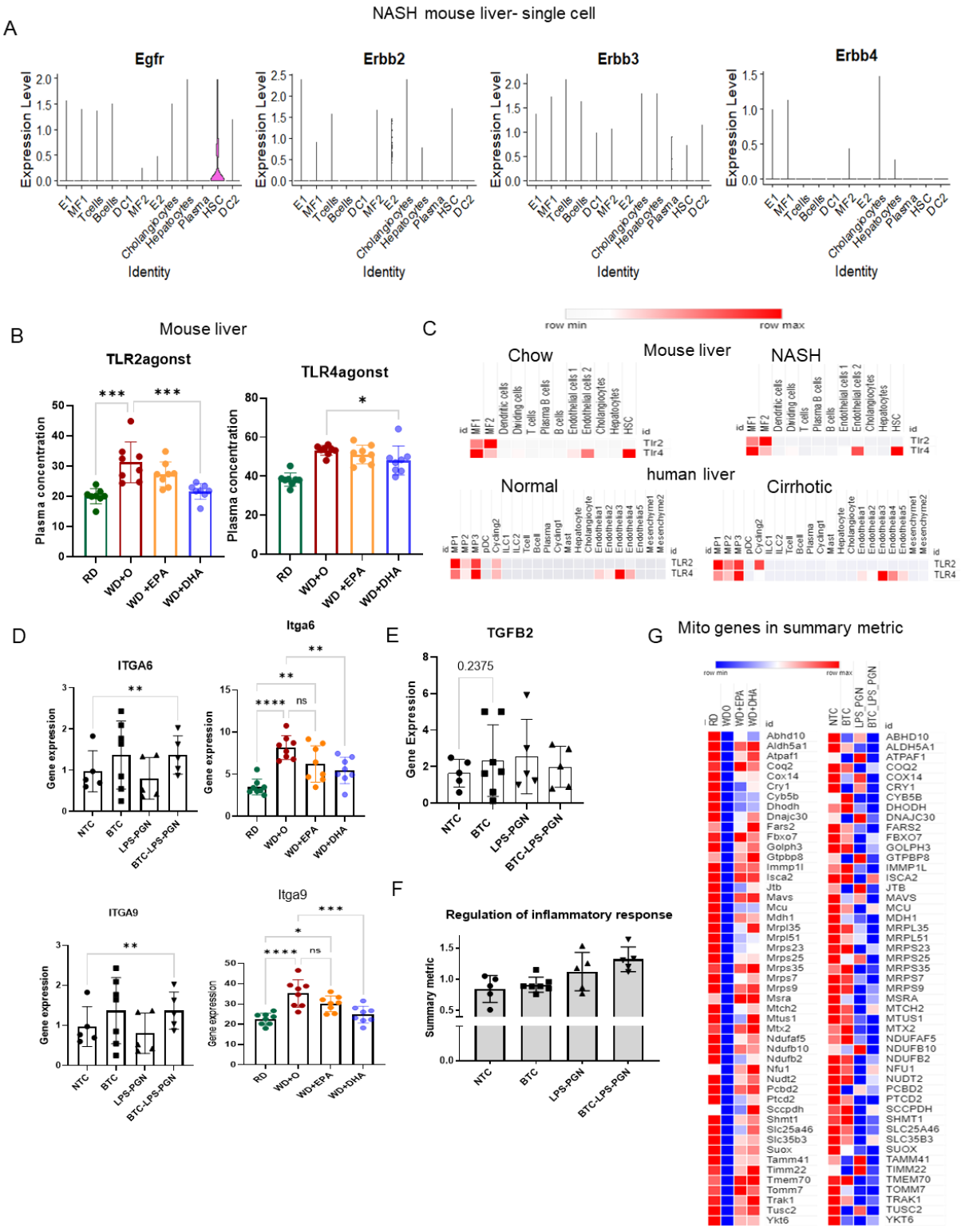

bioRxiv preprint doi: https://doi.org/10.1101/2022.10.03.510635; this version posted October 5, 2022. The copyright holder for this preprint (which was not certified by peer review) is the author/funder, who has granted bioRxiv a license to display the preprint in perpetuity. It is made available under aCC-BY 4.0 International license.

Figure 6 suppl

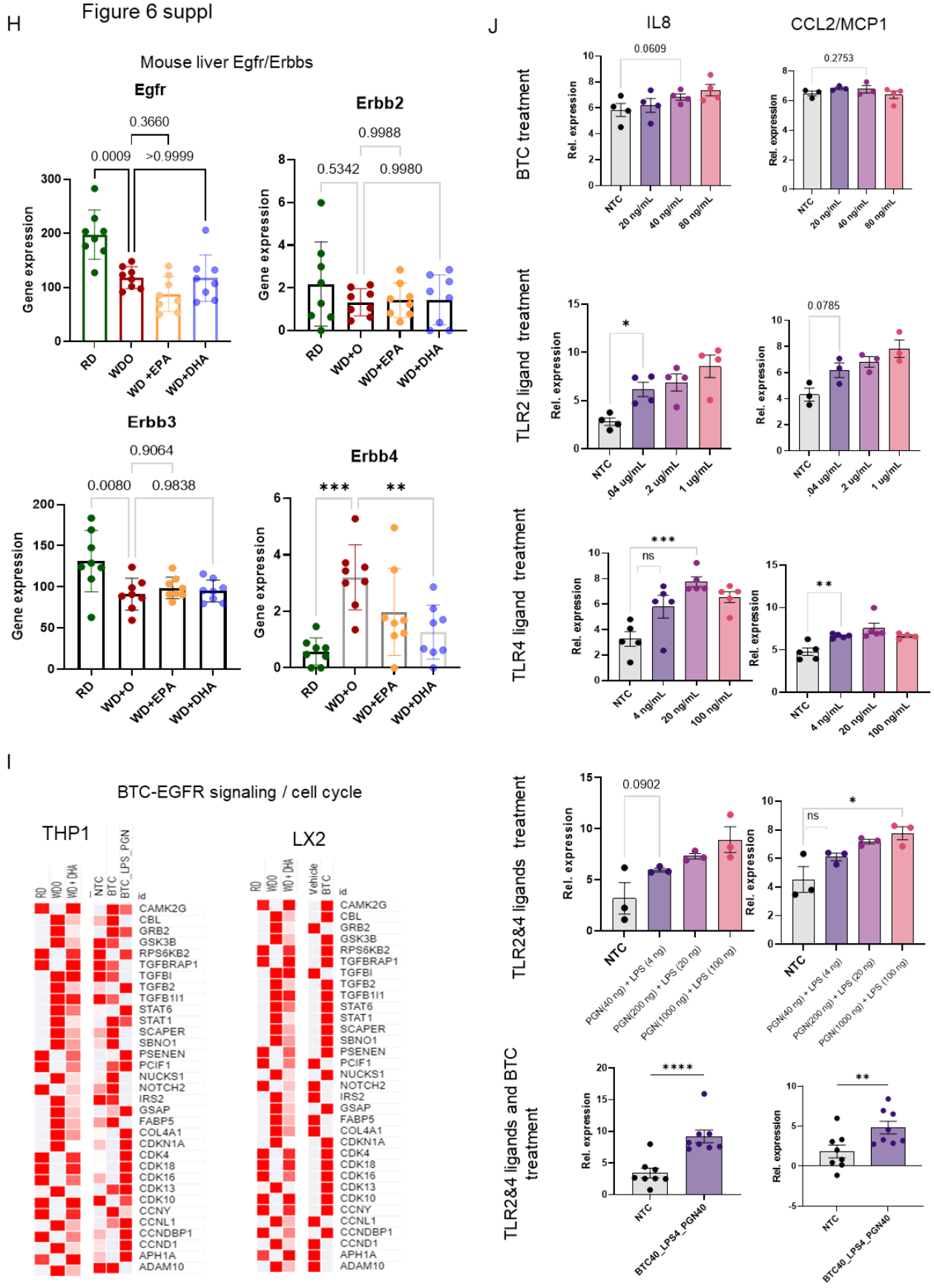

bioRxiv preprint doi: https://doi.org/10.1101/2022.10.03.510635; this version posted October 5, 2022. The copyright holder for this preprint (which was not certified by peer review) is the author/funder, who has granted bioRxiv a license to display the preprint in perpetuity. It is made available under aCC-BY 4.0 International license.

Suppl Figure 6. A. The expression of Egfr and other Erbbs in the NASH mouse model single cell RNA sequence data.
B. Expression of TLR2/4 agonists in the NASH preventive model is shown in bar graphs colored by treatment effects (Ordinary One-way ANOVA, with multiple comparisons test with WD+O, ns (not significant), *p<0.05, ** p<0.001, *** p<0.005, ****p<0.0001)
C. The mouse and human liver (with or without NASH/Cirrhosis) cluster wise average TLR2/4 gene expression from the single cell RNA sequence data. The color scale is indicated from high expression of the genes in red to low in white.
D. The integrin (ITGA6 and ITGA9) expression in the NASH preventive model is shown in bar graphs colored by treatment effects (Ordinary One-way ANOVA, with multiple comparisons test with WD+O, ns (not significant), *p<0.05, ** p<0.001, *** p<0.005, ****p<0.0001) and in THP-1 cells treated with BTC and or TLR2/4 ligands (20 ng/ml; 5 separate experiments, paired, one-sided t-test, ns (not significant), *p<0.05).
E. Normalized TGFβ-2 expression in THP-1 cells treated with BTC and or TLR2/4 ligands (20 ng/ml; 5 separate experiments, paired, one-sided t-test, ns (not significant), *p<0.05).
F. A summary metric bar graph for BTC/TLR2/4 ligand treatment effects in THP1 cells revered by DHA treatment in vivo model from the enrichment analysis.
G. A heatmap from gene list of mitochondria in summary metric for BTC/TLR2/4 ligand treatment effects in THP1 cells revered by DHA treatment in vivo model from the enrichment analysis. The color scale is indicated from high expression of the genes in red to low in blue.
H. The Egfr/Erbbs expression in the NASH preventive model is shown in bar graphs colored by treatment effects (Ordinary One-way ANOVA, with multiple comparisons test with WD+O, ns (not significant), *p<0.05, ** p<0.001, *** p<0.005, ****p<0.0001)
I. The gene expression heatmap from BTC/TLR2/4 ligands treated THP-1 and LX2 cells shows genes involved in EGFR pathway and cell cycle pathway are induced. These set of genes were revered by DHA in the mouse model. The color scale in heatmap is indicated from high expression of the genes in red to low in white.
J. The dose-response standardization experiments with series of concentrations of BTC, TLR2/4 ligands on THP-1 cells before identifying the lowest concentration for combination of all three together. The well-known cytokines were chosen as markers of gene expression with treatments (IL6 and CCL2; 5 separate experiments, paired, one-sided t-test, ns (not significant), *p<0.05, ** p<0.001, *** p<0.005, ****p<0.0001).

Materials and Methods

Animals and diets

Study design for DHA mediated NASH prevention and remission in Male *Ldlr* $^{-/-}$ mice.
This study was carried out in strict accordance with the recommendations in the Guide for Care and Use of Laboratory animals of the National Institutes of Health. All procedures for the use and care of animals for laboratory research were approved by the Institutional Animal Care and Use Committee at Oregon state University (Permit number: A3229-01). Anthropometric, plasma and liver samples used in this study were obtained from our previously published NASH prevention and treatment studies (*12*, *25*). Briefly, male mice (B6:129S7-Ldlr$^{tmHer/j}$, stock# 002207) were purchased from Jackson Labs and were group housed (4 mice/cage) and maintained on a 12-hour light/dark cycle. Mice were acclimatized to the Oregon State University Linus Pauling science center vivarium for 2 weeks before proceeding with the experiments.
NASH Prevention Study: This study was designed to determine if EPA and DHA differed in their capacity to prevent western diet-induced NASH (*12*). Mice consumed the one of the following 5 diets, ad libitum for 16 weeks; each group consisted of 8 male mice. Purina chow 5001 consisting of 13.5% energy as fat and 58.0% energy as carbohydrates was used as the Reference diet (**RD**). The western diet (**WD**) was obtained from Research Diets (12709B) and used to induce NASH. The WD consisted of 17% energy as protein, 43% energy as carbohydrate, and 41% energy as fat; cholesterol was at 0.2% wt:wt. The WD was supplemented with olive oil (**WDO**), eicosapentaenoic acid (**WD + EPA**), docosahexaenoic acid (**WD + DHA**), or both EPA and EHA (**WD + EPA + DHA**). EPA and DHA were added to the diets to

bioRxiv preprint doi: https://doi.org/10.1101/2022.10.03.510635; this version posted October 5, 2022. The copyright holder for this preprint (which was not certified by peer review) is the author/funder, who has granted bioRxiv a license to display the preprint in perpetuity. It is made available under aCC-BY 4.0 International license.

yield 2% of total calories; for the EPA + DHA, each was added to yield 1% of total calories, i.e. 2% total calories as $C_{20\text{-}22}$ ω3 PUFA. OO was added to the WD to have a uniform level of fat energy in all the WDs. Preliminary studies established that the addition of OO had no effect on diet-induced fatty liver disease in *Ldlr*$^{-/-}$ mice. EPA was purchased from Futurebiotics as Newharvest EPA, a DuPont product, while DHA was obtained as a generous gift from DSM, formally Martek Bioscience). The amount of EPA or DHA added to the diets is equivalent to the amount prescribed for treating patients for hypertriglyceridemia (*79, 80*). At the end of the 16-week feeding trial, mice were euthanized with CO2, blood (RBC and plasma) and liver were collected and stored at -80^{o}C for later extractions of RNA, lipids, proteins.

NASH Treatment Study: This study was designed to assess the capacity of DHA to reverse the effects of WD-induced NASH (*41*). As such, male Ldlr $^{-/-}$ mice were fed the WD for 22 wks. These mice were separated into 2 groups: one group was maintained on a WD + olive oil, with the other group was maintained on the WD + DHA. The diet composition was as described above for the prevention study. Both groups were euthanized after 8 wks of these diets. A control group was maintained on the RD for 30 wks. At the end of the study, mice were euthanized, and samples collected and processed as above.

Cell culture

LX2 cells were obtained from SL Friedman (Mount Sani Medical School) (*46*). LX2 cells are activated human hepatic stellate cells; they were maintained in DMEM with 10% FCS containing penicillin and streptomycin. Cells were plated onto 100 mm plastic petri dishes ~100,000 cells/plate and treated with fatty acids (at 50 μM) in endotoxin-free BSA (at 20 μM) during the growth phase. Fatty acids [oleic acid (18:1 ω9) and DHA (22:6, ω3); Nu-Chek Prep] were used at 50 μM for 2- 48-hour cycle treatments. After this pre-treatment, cells were trypsinized, washed in PBS, counted and plated at 3000 cells/well in a 96-well plate. Cells were fed DMEM with 1 % FCS without or with betacellulin (human recombinant betacellulin (BTC), R&D Systems) for 72 hrs; the concentration ranged from 1.25 to 25 ng/ml. At the completion of BTC treatment, media was removed, washed with PBS and DNA/well was quantified using the CyQuant cell proliferation assay (Thermofisher); DNA fluoresces was quantified [excitation at 485 nm & emission at 530 nm. This experiment was repeated 3 times.

Collagen Production: Pico Sirius red quantitation of collagen production: Cells were pretreated with fatty acids as described above, trypsinized, counted and plated onto 12-well cell culture plates at 80,000 cells/well in DMEM +1% FCS and treated without and with 20 ug/ml BTC for72 hrs. At the end of treatment, media was removed, cells were washed with PBS and stained with pico Sirius Red (Abcam) for 2 hrs at room temperature. After staining cells were washed with an acetic acid solution, photographed and the stain was removed using 50 mM NaOH. The level of staining per well was quantified at 540 nm. The level of protein/well was quantified after solubilizing the protein in 50 mM NaOH and using the Pierce BSA kit. This experiment was repeated 4 times.

Cell Vitality: Alamar Blue (Creative Labs) assessment of cell vitality (NADH conversion to NAD^{+}): Using the protocol describe above, we assessed the vitality of cells after treatment with fatty acids and BTC. Alamar blue (50 μl/1.0 ml media) was added to the cells and fluorescence was measured at 590 nm 4 hrs after Alamar Blue addition.

RNASeq: RNA was extracted from LX2 cells using Trizol (Invitrogen) as previously described (*25*) from cells treated with fatty acids (oleic acid and DHA at 50 μM for 72 hrs) as described above. Cells were seeded onto 6-well plates at 40,000 cells/well; and cells were treated with fatty acids for 96 hrs as describe above. Afterward, media was removed, and cells were

bioRxiv preprint doi: https://doi.org/10.1101/2022.10.03.510635; this version posted October 5, 2022. The copyright holder for this preprint (which was not certified by peer review) is the author/funder, who has granted bioRxiv a license to display the preprint in perpetuity. It is made available under aCC-BY 4.0 International license.

treated without and with BTC at 20 ng/ml for 72 hrs. Cells were harvested for RNA extraction (Triazol). cDNA was prepared for RNASeq analysis as described.

THP-1 cells

BTC and TLR co-stimulation

THP-1 monocytes were cultured in RPMI 1640 medium adjusted to contain 4.5 g/L glucose and supplemented with 1% Penicillin/Streptomycin, 10% FBS, 1 mM sodium pyruvate, 10 mM HEPES. For experiments, monocytes were first seeded in 24 well plates at 400,000 cells/well in 1 mL of complete medium with 50 ng/mL PMA (phorbol 12-myristate 13-acetate) to induce polarization, for 24 hours. Then, attached cells were washed with sterile PBS to remove residual serum and PMA containing media. Cells were stimulated with a TLR2 agonist at 40 ng/mL (PGN-BS, Invivogen, San Diego, CA), TLR4 agonist at 4 ng/mL (LPS-B5, Invivogen, San Diego, CA), BTC at 40 ng/mL (human recombinant Betacellulin protein, R&D systems, MN), or combinations of all for 6 hours. Treatments were prepared in serum-free semi-complete RPMI 1640 media (see above for other components) supplemented with 20 µM BSA and 50 µM BHT (Butylated hydroxytoluene). Cells were lysed with 300 µL RLT buffer (Qiagen) and cell lysates were stored at -80 ºC.

Primers

qRT-PCR data analysis

THP-1 cells' response to TLR and BTC stimulation was assessed by qRT-PCR. Briefly, raw Cycle Threshold (CT) values from the StepOnePlus Real Time PCR instrument for genes of interest were normalized to CT values of a housekeeping gene, TMEM59, by delta CT method and relativized by $2^{-\Delta CT}$. Data were then median normalized and Log_2 transformed before being plotted in GraphPad Prism 9.

Gene	Forward	Reverse	Organism
IL8	ACTCCAAACCTTTCCACCCCA	CCCTCTGCACCCAGTTTTCCT	Human
TMEM59	GCTTCATAACCTCTTCATGGAC	GGATTTCTGGCTTAGACTGGA	Human
CCL2/MCP-1	CCCCAGTCACCTGCTGTTAT	AGATCTCCTTGGCCACAATG	Human

RNA extraction and RNA sequencing library preparation

RNA was extracted from cell lysates using the RNeasy Mini Kit and subjected to a DNase treatment according to manufacturer's protocols (Qiagen) then stored at -80 ºC until further use. mRNA libraries were prepared for sequencing with the Lexogen QuantSeq 3' mRNA-Seq Library Prep Kit (FWD) HT for Illumina Sequencing platforms (Kit#k15.384) and sequenced on the Illumina NextSeq at Oregon State University.

cDNA and qRT-PCR

cDNA was prepared from 0.5-1ug of RNA via reverse transcription using the qScript XLT cDNA SuperMix kit (Quantabio). qRT-PCR was performed for gene expression using the AzuraView GreenFast qPCR Blue Mix HR (Azura Genomics). 96-well plates were prepared with 10 ng of cDNA in triplicate reactions for each gene and sample and run on an Applied Biosystems StepOnePlus Real Time PCR instrument.

Sequencing of RNA (RNAseq)

RNA libraries were prepared with the QuantSeq 3'mRNA-Seq Library Prep Kit (Lexogen) for the Apollo 324 NGS Library Prep System and sequenced using Illumina NextSeq. The sequences were processed to remove the adapter, polyA and low-quality bases by BBTools (https://jgi.doe.gov/data-and-tools/bbtools/) using bbduk parameters of k=13, ktrim=r,

bioRxiv preprint doi: https://doi.org/10.1101/2022.10.03.510635; this version posted October 5, 2022. The copyright holder for this preprint (which was not certified by peer review) is the author/funder, who has granted bioRxiv a license to display the preprint in perpetuity. It is made available under aCC-BY 4.0 International license.

forcetrimleft=12, useshortkmers=t, mink=5, qtrim=r, trimq=15, minlength=20. Then the reads were aligned to mouse genome and transcriptome (ENSEMBL NCBIM37) using Tophat (v2.1.1) with default parameters. The number of reads per million for mouse liver genes were counted using HTSeq (v 0.6.0) and quantile normalized. Cell lines sequencing/analysis was performed similarly, but with the bbduk parameters of k=13, ktrim=r, forcetrimleft=11, useshortkmers=t, mink=5, qtrim=r, trimq=10, minlength=20. The reads were aligned to the human genome and transcriptome (Gencode v40) using STAR v2.5.3a. BRB-ArrayTools was used to identify differentially expressed genes between treatments.

Metabolomic and Lipidomic

Data were prepared, and analysis were carried out from the NASH Prevention study and Treatment study. Hepatic lipids were extracted and subject to UPLC/MS/MS analysis as previously described (*81*) with modifications described in Materials and methods.

Treatment categorization of omics data

The genes and other parameters whose expressions or values are significantly changed by WD (FDR<10%) were considered for treatment effects. Out of these parameters and genes, those that have treatment effect reversal with a P-value<0.05 were categorized as DHA if uniquely DHA (opposite to WD+O/ND & WD+DHA/WD+O P-value<0.05), uniquely EPA (opposite to WD+O/ND & WD+EPA /WD+O P-value<0.05), similar in both EPA&DHA (opposite to WD+O/ND & both WD+EPA /WD+O and WD+DHA/WD+O, P-value<0.05) and with no treatment effect (NA; with both WD+EPA /WD+O and WD+DHA/WD+O, P-value>0.05). To be consistent with many previous studies, the treatment effects were also tested in the combination of preventive treatment though not used further in the analysis (EPA+DHA; WD+EPA+DHA /WD+O, P-value<0.05).

Reconstructing the NASH liver multi-omics network

The network reconstruction was carried out as described in the previous papers from our group with minor dataset specific modifications (*26, 34*). The genes and other parameters whose expressions or values are significantly changed by WD (FDR<10%) were chosen for constructing the NASH network. First, from liver tissue between all pairs of genes (GE) and metabolic parameters (phenotypes, P) spearman rank correlations were calculated by pooling the samples per diet (WD+O, WD+EPA and WD+DHA). Meta-analysis was performed to retain edges with same sign of correlation coefficient in all three diets. Edges were furthered filtered by the following criteria: individual p-value of correlation within each diet from pooled experiments <20%, combined Fisher's p-value over diets from pooled experiments <5% and FDR cutoff of 10% for edges within tissues and for phenotypes and between lipidomic, metabolomic and plasma biochemicals and edges needed to satisfy principles of causality [i.e., satisfied fold change relationship between the two partners in the WD+O vs. ND comparison]. Next, correlations were calculated per diet for the experiment pairwise between parameters (Gene Expression + Lipidomic and Metabolomic data (LM)) and (P+LM). Finally, edges obtained from pooling were retained if they had the same sign of correlation coefficient as in 3 groups (3 diets, WD+O, WD+EPA and WD+DHA). False positive edges while pooling the different diets were removed in the creation of the network. The proportion of genes, metabolites and lipids that made it to the final network (following statistical cutoffs) was determined after applying selection for significance in differentially expressed parameters in liver prior to applying correlation cutoffs.

Single cell RNA sequence data analysis

Datasets

bioRxiv preprint doi: https://doi.org/10.1101/2022.10.03.510635; this version posted October 5, 2022. The copyright holder for this preprint (which was not certified by peer review) is the author/funder, who has granted bioRxiv a license to display the preprint in perpetuity. It is made available under aCC-BY 4.0 International license.

Single cell dataset (GSE129516) for mouse NASH model was obtained from single cell RNA-sequence on non-parenchymal cells of healthy vs NASH mouse liver. These are then reanalyzed and used in our multi-omics network analysis to infer liver cell types.
Human liver single cell RNA sequencing data (GSE136103) from normal and Cirrhosis patients were reanalyzed.

scRNA sequence analysis

The raw gene expression matrix (UMI counts per gene per cell in the liver tissue) was filtered, normalized, and clustered using a standard Seurat version 3.1.0 in R [https://www.R-project.org/] (*82*). Cell and gene filtering were performed as mentioned in previous publications. During quality filtering, cells with a very small library size (<5000) and a very high (>12%) mitochondrial genome transcripts were removed. The genes detected (UMI count > 0) in less than three cells were also removed from further processes. Then log normalization and further clustering is performed using standard Seurat package procedures. Principal component analysis was used to reduce dimensions that represent cell clusters. The number of components from this analysis used for the elbow of a scree plot, which further aid in selecting the significant clusters. The different cell type clusters in a sample were visualized using t-distributed Stochastic Neighbor Embedding of the principal components as implemented in Seurat. The liver tissue specific cell-type identities for each cluster were determined manually using a compiled panel of available immune and other cell specific marker expression as per the previously published papers (*28, 30*).

Single cell RNA sequence for assignment of gene in the NASH network to a specific cell type

The normalized UMI > 1.0, with a fold change significantly and uniquely expressed genes in a cell specific cluster were then assigned to that specific set of genes in the network to indicate they belong to that specific cell type. It is the primary rule to assign a gene to a cell type. Next, higher expression in the cell cluster (and optional fold change (log2FC >0.25, p value <0.05) for a gene gets assigned with that specific cell type for the tissue. Here ranking by average expression for each gene in the clusters helps to determine its cluster specificity by the higher expression in that cell type than another in the whole tissue. This is implemented for evaluating highest cell cluster average expression of a gene, among all other cell clusters in network.

Detecting subnetworks and functional enrichment

Infomap (mapequation.org) was used to identify subnetworks using the default commands. Functional enrichment of clusters was then performed using metascape (http://metascape.org) (*83*).

Identifying of key nodes between subnetworks using BiBC analysis

Analysis of networks was performed using the python package NetworkX v2.2. Bipartite betweenness centrality (BiBC) was calculated between all pairs (66 total) of the twelve clusters previously identified by Infomap. The nodes were then ranked by their resulting BiBC and scaled to range of 0-100. BiBC was also calculated and scaled similarly between all genes and anthropometric data.

Creation and analysis of random networks

Random networks were created similar to as was described in Kahalehili et al., 2021 (*84*). Briefly, 5,000 Erdos-Renyi random networks were created, utilizing the same number of nodes and edges that were present in the real, reconstructed network. BiBC was calculated both 1) between DHA controlled genes and anthropometric nodes and 2) between DHA controlled genes and DHA controlled metabolomic/lipidomic data. Plotly (https://chart-

bioRxiv preprint doi: https://doi.org/10.1101/2022.10.03.510635; this version posted October 5, 2022. The copyright holder for this preprint (which was not certified by peer review) is the author/funder, who has granted bioRxiv a license to display the preprint in perpetuity. It is made available under aCC-BY 4.0 International license.

studio.plotly.com/create/#/) was used to create the 2D contour histograms for visualization of the random network results.

Cardiolipin network

The cardiolipin network was constructed as we modeled the multi-omics network described above. Lipids such as PAs and PGs in the top BiBC in the Multiomics network were precursors of Cardiolipins specifically known to be part of mitochondrial membrane. The genes part of synthesis and remodeling the cardiolipin were also part of the top BiBC in the network such as Lpgat1, Prelid3b and Taz. Therefore, a module of subnetwork among all these components of Cardiolipin synthesis and remodeling was reconstructed from the NASH network model to detail this process. To have a complete model, additional enzymes in the pathway were incorporated to the model and correlations to the rest of the module were calculated though they were not highly statistically significant in the above multi-omics network model. Except Pla2g1b, which got filtered out, all other 18 genes could be part of the cardiolipin network. Additionally, treatment effects were estimated for the genes and lipids (PAs and PGs) as part of cardiolipin network analysis.

Intrahepatic ligand-receptor interaction network

The knowledgebase of ligand receptor interaction information available for mouse genes (*85*), was overlayed on to reconstructed NASH Multiomics network genes. Additionally, this allowed the interrogation of ligand-receptor network with respect to each cell in the network that a gene can be represented as ligand or receptor.

Human liver cancer meta-analysis

Human cancer data from hepatic cellular cancer (HCC) and cholangiocytes cancer (CC) were selected from GEO data sets (GSE14520, GSE26566, GSE102079, GSE56140, GSE98617, GSE76427, GSE84005). Meta-analysis using RankProd method described in the publicly available tool OMiCC (*86*) was carried out for these 7 sets of data with 32 healthy, 260 non-tumor samples and 544 tumor samples (Suppl Figure 4A). At first sample sets of both tumor types were compared against their respective paired non-tumor or healthy samples. Additionally, a standard Fisher approach of meta-analysis was also carried out and an overlapping set of genes were selected.

Then a signature set of genes were identified by matching (among orthologous) genes between mouse and human using Biomart (*87*) for the concordant fold change direction as WD+O/RD in the NASH network model and genes that are significant with FDR less than 15% and Fisher p value less than 5%.

The human liver cancer meta-analysis signature genes were overlapped with the NASH mouse model network genes with treatment effects to identify further subset of genes.

Gene Ontology analyses

The gene ontology and functional enrichment were carried out using Metascape and innateDB (*83, 88*) with mouse or human reference databases. The reference database is determined depending on the species of the specific data in question.

Pathway summary metric

Using published approach(*89*) with minor adaptions described in our previous papers(*90, 91*), each top gene ontology pathway enriched in the THP-1 experiment (with BTC and TLR ligands and revered by DHA preventive model significantly in the Multiomics network) was recognized and the gene belong to the pathways were identified. Using median normalization, a value for each gene in each treatment replicate and then additionally using their median, summary metric

bioRxiv preprint doi: https://doi.org/10.1101/2022.10.03.510635; this version posted October 5, 2022. The copyright holder for this preprint (which was not certified by peer review) is the author/funder, who has granted bioRxiv a license to display the preprint in perpetuity. It is made available under aCC-BY 4.0 International license.

was calculated for the individual pathway. A paired t-test between normal and treatment condition were performed to evaluate significance.

Statistical analysis

In mouse studies data are expressed as geometric mean of replicates. Data are shown as the mean ± standard deviation in animal studies and *in vitro* experiments. Group comparisons were performed using an unpaired *t* test and Ordinary One-way analysis of variance (ANOVA), followed by Tukey's *post hoc* or Dunnett's multiple comparisons tests, where $p < 0.05$ indicates statistical significance. In cell line and RNA sequence analysis, comparisons between groups were performed using Student's *t* test or the Mann-Whitney *U* test and Kruskal-Wallis test when appropriate. Categorical variables are shown as counts and percentages. Differences between categorical variables were assessed with the chi-squared test or Fisher's exact test. Spearman's rank correlation rho coefficients were calculated for network edges between all parameters using R statistical packages. Details of statistical analyses are described additionally in the corresponding figure legends. GraphPad Prism 9 was used for all analyses.

bioRxiv preprint doi: https://doi.org/10.1101/2022.10.03.510635; this version posted October 5, 2022. The copyright holder for this preprint (which was not certified by peer review) is the author/funder, who has granted bioRxiv a license to display the preprint in perpetuity. It is made available under aCC-BY 4.0 International license.

References

1. M. A. Konerman, J. C. Jones, S. A. Harrison, Pharmacotherapy for NASH: Current and emerging. *J Hepatol* **68**, 362-375 (2018).
2. J. F. Dufour *et al.*, Current therapies and new developments in NASH. *Gut* **71**, 2123-2134 (2022).
3. J. V. Lazarus *et al.*, Advancing the global public health agenda for NAFLD: a consensus statement. *Nat Rev Gastroenterol Hepatol* **19**, 60-78 (2022).
4. T. Marjot, A. Moolla, J. F. Cobbold, L. Hodson, J. W. Tomlinson, Nonalcoholic Fatty Liver Disease in Adults: Current Concepts in Etiology, Outcomes, and Management. *Endocr Rev* **41**, (2020).
5. D. B. Jump, C. M. Depner, S. Tripathy, K. A. Lytle, Potential for dietary ω-3 fatty acids to prevent nonalcoholic fatty liver disease and reduce the risk of primary liver cancer. *Adv Nutr* **6**, 694-702 (2015).
6. J. Ampuero *et al.*, Systematic review and meta-analysis: analysis of variables influencing the interpretation of clinical trial results in NAFLD. *J Gastroenterol* **57**, 357-371 (2022).
7. B. A. Neuschwander-Tetri, Therapeutic Landscape for NAFLD in 2020. *Gastroenterology* **158**, 1984-1998.e1983 (2020).
8. D. Pfister *et al.*, NASH limits anti-tumour surveillance in immunotherapy-treated HCC. *Nature* **592**, 450-456 (2021).
9. M. Fridén *et al.*, Hepatic Unsaturated Fatty Acids Are Linked to Lower Degree of Fibrosis in Non-alcoholic Fatty Liver Disease. *Front Med (Lausanne)* **8**, 814951 (2021).
10. P. A. Burke, P. R. Ling, R. A. Forse, B. R. Bistrian, Conditionally essential fatty acid deficiencies in end-stage liver disease. *Nutrition* **15**, 302-304 (1999).
11. C. M. Depner *et al.*, A metabolomic analysis of omega-3 fatty acid-mediated attenuation of western diet-induced nonalcoholic steatohepatitis in LDLR-/- mice. *PLoS One* **8**, e83756 (2013).
12. C. M. Depner, K. A. Philbrick, D. B. Jump, Docosahexaenoic acid attenuates hepatic inflammation, oxidative stress, and fibrosis without decreasing hepatosteatosis in a Ldlr(-/-) mouse model of western diet-induced nonalcoholic steatohepatitis. *J Nutr* **143**, 315-323 (2013).
13. M. H. Spooner, D. B. Jump, Omega-3 fatty acids and nonalcoholic fatty liver disease in adults and children: where do we stand? *Curr Opin Clin Nutr Metab Care* **22**, 103-110 (2019).
14. A. Iannelli *et al.*, Preoperative 4-week supplementation with omega-3 polyunsaturated fatty acids reduces liver volume and facilitates bariatric surgery in morbidly obese patients. *Obes Surg* **23**, 1761-1765 (2013).
15. D. B. Jump, K. A. Lytle, C. M. Depner, S. Tripathy, Omega-3 polyunsaturated fatty acids as a treatment strategy for nonalcoholic fatty liver disease. *Pharmacol Ther* **181**, 108-125 (2018).
16. S. Gutiérrez, S. L. Svahn, M. E. Johansson, Effects of Omega-3 Fatty Acids on Immune Cells. *Int J Mol Sci* **20**, (2019).

bioRxiv preprint doi: https://doi.org/10.1101/2022.10.03.510635; this version posted October 5, 2022. The copyright holder for this preprint (which was not certified by peer review) is the author/funder, who has granted bioRxiv a license to display the preprint in perpetuity. It is made available under aCC-BY 4.0 International license.

17. J. Yang *et al.*, Oxidative Stress and Non-Alcoholic Fatty Liver Disease: Effects of Omega-3 Fatty Acid Supplementation. *Nutrients* **11**, (2019).
18. H. Watson *et al.*, A randomised trial of the effect of omega-3 polyunsaturated fatty acid supplements on the human intestinal microbiota. *Gut* **67**, 1974-1983 (2018).
19. V. Šmíd *et al.*, Effect of Omega-3 Polyunsaturated Fatty Acids on Lipid Metabolism in Patients With Metabolic Syndrome and NAFLD. *Hepatol Commun* **6**, 1336-1349 (2022).
20. L. Hodson *et al.*, Docosahexaenoic acid enrichment in NAFLD is associated with improvements in hepatic metabolism and hepatic insulin sensitivity: a pilot study. *Eur J Clin Nutr* **71**, 973-979 (2017).
21. K. Musa-Veloso *et al.*, Systematic review and meta-analysis of controlled intervention studies on the effectiveness of long-chain omega-3 fatty acids in patients with nonalcoholic fatty liver disease. *Nutr Rev* **76**, 581-602 (2018).
22. D. Tobin, M. Brevik-Andersen, Y. Qin, J. K. Innes, P. C. Calder, Evaluation of a High Concentrate Omega-3 for Correcting the Omega-3 Fatty Acid Nutritional Deficiency in Non-Alcoholic Fatty Liver Disease (CONDIN). *Nutrients* **10**, (2018).
23. L. Okada *et al.*, Omega-3 PUFA modulate lipogenesis, ER stress, and mitochondrial dysfunction markers in NASH - Proteomic and lipidomic insight. *Clin Nutr* **37**, 1474-1484 (2018).
24. E. Zöhrer *et al.*, Efficacy of docosahexaenoic acid-choline-vitamin E in paediatric NASH: a randomized controlled clinical trial. *Appl Physiol Nutr Metab* **42**, 948-954 (2017).
25. K. A. Lytle, C. M. Depner, C. P. Wong, D. B. Jump, Docosahexaenoic acid attenuates Western diet-induced hepatic fibrosis in Ldlr-/- mice by targeting the TGFβ-Smad3 pathway. *J Lipid Res* **56**, 1936-1946 (2015).
26. X. Dong *et al.*, Reverse enGENEering of Regulatory Networks from Big Data: A Roadmap for Biologists. *Bioinform Biol Insights* **9**, 61-74 (2015).
27. A. Yambartsev *et al.*, Unexpected links reflect the noise in networks. *Biol Direct* **11**, 52 (2016).
28. X. Xiong *et al.*, Landscape of Intercellular Crosstalk in Healthy and NASH Liver Revealed by Single-Cell Secretome Gene Analysis. *Mol Cell* **75**, 644-660.e645 (2019).
29. J. S. Seidman *et al.*, Niche-Specific Reprogramming of Epigenetic Landscapes Drives Myeloid Cell Diversity in Nonalcoholic Steatohepatitis. *Immunity* **52**, 1057-1074.e1057 (2020).
30. P. Ramachandran *et al.*, Resolving the fibrotic niche of human liver cirrhosis at single-cell level. *Nature* **575**, 512-518 (2019).
31. A. Morgun *et al.*, Uncovering effects of antibiotics on the host and microbiota using transkingdom gene networks. *Gut* **64**, 1732-1743 (2015).
32. T. R. Sorrells, A. D. Johnson, Making sense of transcription networks. *Cell* **161**, 714-723 (2015).
33. S. Choobdar *et al.*, Assessment of network module identification across complex diseases. *Nat Methods* **16**, 843-852 (2019).
34. Z. Li *et al.*, Microbiota and adipocyte mitochondrial damage in type 2 diabetes are linked by Mmp12+ macrophages. *J Exp Med* **219**, (2022).

bioRxiv preprint doi: https://doi.org/10.1101/2022.10.03.510635; this version posted October 5, 2022. The copyright holder for this preprint (which was not certified by peer review) is the author/funder, who has granted bioRxiv a license to display the preprint in perpetuity. It is made available under aCC-BY 4.0 International license.

35. C. D. Green, C. G. Ozguden-Akkoc, Y. Wang, D. B. Jump, L. K. Olson, Role of fatty acid elongases in determination of de novo synthesized monounsaturated fatty acid species. *J Lipid Res* **51**, 1871-1877 (2010).
36. A. F. Anzmann *et al.*, Diverse mitochondrial abnormalities in a new cellular model of TAFFAZZIN deficiency are remediated by cardiolipin-interacting small molecules. *J Biol Chem* **297**, 101005 (2021).
37. J. Dudek, Role of Cardiolipin in Mitochondrial Signaling Pathways. *Front Cell Dev Biol* **5**, 90 (2017).
38. G. Oemer *et al.*, Phospholipid Acyl Chain Diversity Controls the Tissue-Specific Assembly of Mitochondrial Cardiolipins. *Cell Rep* **30**, 4281-4291.e4284 (2020).
39. E. L. Van Blarigan *et al.*, Marine ω-3 Polyunsaturated Fatty Acid and Fish Intake after Colon Cancer Diagnosis and Survival: CALGB 89803 (Alliance). *Cancer Epidemiol Biomarkers Prev* **27**, 438-445 (2018).
40. E. Dierge *et al.*, Peroxidation of n-3 and n-6 polyunsaturated fatty acids in the acidic tumor environment leads to ferroptosis-mediated anticancer effects. *Cell Metab* **33**, 1701-1715.e1705 (2021).
41. K. A. Lytle, C. P. Wong, D. B. Jump, Docosahexaenoic acid blocks progression of western diet-induced nonalcoholic steatohepatitis in obese Ldlr-/- mice. *PLoS One* **12**, e0173376 (2017).
42. M. J. Wieduwilt, M. M. Moasser, The epidermal growth factor receptor family: biology driving targeted therapeutics. *Cell Mol Life Sci* **65**, 1566-1584 (2008).
43. J. Chen *et al.*, Expression and Function of the Epidermal Growth Factor Receptor in Physiology and Disease. *Physiol Rev* **96**, 1025-1069 (2016).
44. M. A. Olayioye, R. M. Neve, H. A. Lane, N. E. Hynes, The ErbB signaling network: receptor heterodimerization in development and cancer. *Embo j* **19**, 3159-3167 (2000).
45. J. K. Carter, S. L. Friedman, Hepatic Stellate Cell-Immune Interactions in NASH. *Front Endocrinol (Lausanne)* **13**, 867940 (2022).
46. L. Xu *et al.*, Human hepatic stellate cell lines, LX-1 and LX-2: new tools for analysis of hepatic fibrosis. *Gut* **54**, 142-151 (2005).
47. T. Sun *et al.*, TGFβ2 and TGFβ3 isoforms drive fibrotic disease pathogenesis. *Sci Transl Med* **13**, (2021).
48. K. Miura *et al.*, Toll-like receptor 2 and palmitic acid cooperatively contribute to the development of nonalcoholic steatohepatitis through inflammasome activation in mice. *Hepatology* **57**, 577-589 (2013).
49. L. Wu *et al.*, Anti-toll-like receptor 2 antibody ameliorates hepatic injury, inflammation, fibrosis and steatosis in obesity-related metabolic disorder rats via regulating MAPK and NF-κB pathways. *Int Immunopharmacol* **82**, 106368 (2020).
50. A. Spruss *et al.*, Toll-like receptor 4 is involved in the development of fructose-induced hepatic steatosis in mice. *Hepatology* **50**, 1094-1104 (2009).
51. H. Lanaya *et al.*, EGFR has a tumour-promoting role in liver macrophages during hepatocellular carcinoma formation. *Nat Cell Biol* **16**, 972-977 (2014).
52. L. Shi *et al.*, Regulatory mechanisms of betacellulin in CXCL8 production from lung cancer cells. *J Transl Med* **12**, 70 (2014).

bioRxiv preprint doi: https://doi.org/10.1101/2022.10.03.510635; this version posted October 5, 2022. The copyright holder for this preprint (which was not certified by peer review) is the author/funder, who has granted bioRxiv a license to display the preprint in perpetuity. It is made available under aCC-BY 4.0 International license.

53. E. Seki *et al.*, TLR4 enhances TGF-beta signaling and hepatic fibrosis. *Nat Med* **13**, 1324-1332 (2007).
54. V. T. Samuel, G. I. Shulman, Nonalcoholic Fatty Liver Disease as a Nexus of Metabolic and Hepatic Diseases. *Cell Metab* **27**, 22-41 (2018).
55. I. C. M. Simões, A. Fontes, P. Pinton, H. Zischka, M. R. Wieckowski, Mitochondria in non-alcoholic fatty liver disease. *Int J Biochem Cell Biol* **95**, 93-99 (2018).
56. N. Xie *et al.*, NAD(+) metabolism: pathophysiologic mechanisms and therapeutic potential. *Signal Transduct Target Ther* **5**, 227 (2020).
57. D. A. Hume, K. P. MacDonald, Therapeutic applications of macrophage colony-stimulating factor-1 (CSF-1) and antagonists of CSF-1 receptor (CSF-1R) signaling. *Blood* **119**, 1810-1820 (2012).
58. A. D. Dahlén *et al.*, Trends in Antidiabetic Drug Discovery: FDA Approved Drugs, New Drugs in Clinical Trials and Global Sales. *Front Pharmacol* **12**, 807548 (2021).
59. G. Jermendy *et al.*, Persistence to Treatment with Novel Antidiabetic Drugs (Dipeptidyl Peptidase-4 Inhibitors, Sodium-Glucose Co-Transporter-2 Inhibitors, and Glucagon-Like Peptide-1 Receptor Agonists) in People with Type 2 Diabetes: A Nationwide Cohort Study. *Diabetes Ther* **9**, 2133-2141 (2018).
60. D. L. Bhatt *et al.*, Cardiovascular Risk Reduction with Icosapent Ethyl for Hypertriglyceridemia. *N Engl J Med* **380**, 11-22 (2019).
61. A. M. Jastreboff *et al.*, Tirzepatide Once Weekly for the Treatment of Obesity. *N Engl J Med* **387**, 205-216 (2022).
62. M. E. Rinella, Nonalcoholic fatty liver disease: a systematic review. *Jama* **313**, 2263-2273 (2015).
63. J. Wattacheril, D. Issa, A. Sanyal, Nonalcoholic Steatohepatitis (NASH) and Hepatic Fibrosis: Emerging Therapies. *Annu Rev Pharmacol Toxicol* **58**, 649-662 (2018).
64. Q. M. Anstee, H. L. Reeves, E. Kotsiliti, O. Govaere, M. Heikenwalder, From NASH to HCC: current concepts and future challenges. *Nat Rev Gastroenterol Hepatol* **16**, 411-428 (2019).
65. A. Dropmann *et al.*, TGF-β1 and TGF-β2 abundance in liver diseases of mice and men. *Oncotarget* **7**, 19499-19518 (2016).
66. T. A. Wynn, K. M. Vannella, Macrophages in Tissue Repair, Regeneration, and Fibrosis. *Immunity* **44**, 450-462 (2016).
67. X. Zhang *et al.*, Defective Phosphatidylglycerol Remodeling Causes Hepatopathy, Linking Mitochondrial Dysfunction to Hepatosteatosis. *Cell Mol Gastroenterol Hepatol* **7**, 763-781 (2019).
68. R. R. Rodrigues *et al.*, Transkingdom interactions between Lactobacilli and hepatic mitochondria attenuate western diet-induced diabetes. *Nat Commun* **12**, 101 (2021).
69. J. Xin *et al.*, Preventing non-alcoholic fatty liver disease through Lactobacillus johnsonii BS15 by attenuating inflammation and mitochondrial injury and improving gut environment in obese mice. **98**, 6817-6829 (2014).
70. I. Bourgot, I. Primac, T. Louis, A. Noël, E. Maquoi, Reciprocal Interplay Between Fibrillar Collagens and Collagen-Binding Integrins: Implications in Cancer Progression and Metastasis. *Front Oncol* **10**, 1488 (2020).

bioRxiv preprint doi: https://doi.org/10.1101/2022.10.03.510635; this version posted October 5, 2022. The copyright holder for this preprint (which was not certified by peer review) is the author/funder, who has granted bioRxiv a license to display the preprint in perpetuity. It is made available under aCC-BY 4.0 International license.

71. S. K. Agarwal, Integrins and cadherins as therapeutic targets in fibrosis. *Front Pharmacol* **5**, 131 (2014).
72. S. R. Rahman *et al.*, Integrins as a drug target in liver fibrosis. *Liver Int* **42**, 507-521 (2022).
73. C. Costa *et al.*, Gut Microbiome and Organ Fibrosis. *Nutrients* **14**, (2022).
74. Y. He *et al.*, Targeting PI3K/Akt signal transduction for cancer therapy. *Signal Transduct Target Ther* **6**, 425 (2021).
75. S. Chava, S. Bugide, X. Zhang, R. Gupta, N. Wajapeyee, Betacellulin promotes tumor development and EGFR mutant lung cancer growth by stimulating the EGFR pathway and suppressing apoptosis. *iScience* **25**, 104211 (2022).
76. M. Dahlhoff, E. Wolf, M. R. Schneider, The ABC of BTC: structural properties and biological roles of betacellulin. *Semin Cell Dev Biol* **28**, 42-48 (2014).
77. K. Hedegger *et al.*, Unraveling ERBB network dynamics upon betacellulin signaling in pancreatic ductal adenocarcinoma in mice. *Mol Oncol* **14**, 1653-1669 (2020).
78. W. S. Moon *et al.*, Expression of betacellulin and epidermal growth factor receptor in hepatocellular carcinoma: implications for angiogenesis. *Hum Pathol* **37**, 1324-1332 (2006).
79. M. H. Davidson *et al.*, Efficacy and tolerability of adding prescription omega-3 fatty acids 4 g/d to simvastatin 40 mg/d in hypertriglyceridemic patients: an 8-week, randomized, double-blind, placebo-controlled study. *Clin Ther* **29**, 1354-1367 (2007).
80. W. S. Harris *et al.*, Safety and efficacy of Omacor in severe hypertriglyceridemia. *J Cardiovasc Risk* **4**, 385-391 (1997).
81. M. Garcia-Jaramillo *et al.*, Lipidomic and transcriptomic analysis of western diet-induced nonalcoholic steatohepatitis (NASH) in female Ldlr -/- mice. *PLoS One* **14**, e0214387 (2019).
82. T. Stuart *et al.*, Comprehensive Integration of Single-Cell Data. *Cell* **177**, 1888-1902.e1821 (2019).
83. Y. Zhou *et al.*, Metascape provides a biologist-oriented resource for the analysis of systems-level datasets. *Nat Commun* **10**, 1523 (2019).
84. H. M. Kahalehili *et al.*, Dietary Indole-3-Carbinol Activates AhR in the Gut, Alters Th17-Microbe Interactions, and Exacerbates Insulitis in NOD Mice. *Front Immunol* **11**, 606441 (2020).
85. I. Abugessaisa *et al.*, FANTOM enters 20th year: expansion of transcriptomic atlases and functional annotation of non-coding RNAs. *Nucleic Acids Res* **49**, D892-d898 (2021).
86. N. Shah *et al.*, A crowdsourcing approach for reusing and meta-analyzing gene expression data. *Nat Biotechnol* **34**, 803-806 (2016).
87. F. Cunningham *et al.*, Ensembl 2022. *Nucleic Acids Res* **50**, D988-d995 (2022).
88. K. Breuer *et al.*, InnateDB: systems biology of innate immunity and beyond--recent updates and continuing curation. *Nucleic Acids Res* **41**, D1228-1233 (2013).
89. D. M. Levine *et al.*, Pathway and gene-set activation measurement from mRNA expression data: the tissue distribution of human pathways. *Genome Biol* **7**, R93 (2006).
90. B. Koscso *et al.*, Gut-resident CX3CR1(hi) macrophages induce tertiary lymphoid structures and IgA response in situ. *Sci Immunol* **5**, (2020).

bioRxiv preprint doi: https://doi.org/10.1101/2022.10.03.510635; this version posted October 5, 2022. The copyright holder for this preprint (which was not certified by peer review) is the author/funder, who has granted bioRxiv a license to display the preprint in perpetuity. It is made available under aCC-BY 4.0 International license.

91. N. Shulzhenko *et al.*, Crosstalk between B lymphocytes, microbiota and the intestinal epithelium governs immunity versus metabolism in the gut. *Nat Med* **17**, 1585-1593 (2011).